

POLITECNICO DI TORINO

Collegio di Ingegneria Chimica e dei Materiali

**Corso di Laurea Magistrale
in Ingegneria dei Materiali**

A.a. 2020/21

Tesi di Laurea Magistrale

**Characterization of amorphous silicon
carbide thin films recrystallization**



Candidato

SALVADOR Denis

Relatore

Prof. SCALTRITO Luciano

Dicembre 2021

Index

Introduction.....	5
Internship context	6
Internship work and objective.....	8
Chapter 1: Deposition methods.....	9
1.1 Plasma Enhanced CVD – PECVD.....	10
1.2 Sputtering PVD.....	15
Chapter 2: Characterization methods.....	17
2.1 X-ray photoelectron spectroscopy – XPS	18
2.2 Raman spectroscopy	20
2.3 X-ray diffraction – XRD.....	21
2.4 Ellipsometry.....	22
Chapter 3: Experimental work.....	24
3.1 Layer characterisation – as deposited	25
3.2 Heat treatments	35
3.2.1 PECVD samples	35
Chapter 4: Analysis and discussion of results	49
Chapter 5: Conclusions.....	52
Bibliography	54
Appendix.....	56
Wafer 1 surface.....	56
Wafer 2 surface.....	57
Wafer 3 surface.....	58
Wafer 3 after Ar etching	59
PECVD after heat treatments.....	60

Introduction

The peculiar feature that nowadays accompanies our society, and consequently our lives, is definitely the technological progress in all kinds of sectors. The utilisation of innovative materials is an important step in evolution though the optimal exploitation of their properties in specific applications. Clearly, this is made possible by developments in the technological and production processes inherent in this major field of research.

Among the modern materials, silicon carbide (SiC) certainly plays an important role. SiC is a semiconductor with unique chemical, physical and mechanical properties, making it ideal for various fields of application: it is used in the fields of optoelectronics, sensors, thermal dissipation, but also exploited as a structural material and for the creation of protective coatings, both for its high resistance to wear and for its excellent resistance to corrosion. In modern terms, it is in fact the most promising alternative to silicon for high power/high frequency electronics operating in prohibitive conditions such as high temperature, the presence of radiation and aggressive chemical agents, while its biocompatibility opens up new scenarios for applications in the biomedical sector. Furthermore, SiC is certainly a very promising candidate for the development of graphene-based electronics, being one of the reference substrates for graphene growth.

Hence my decision to write my master's thesis on silicon carbide for the realisation of new optical devices: the internship that I carried out at the laboratories (SiMaP) of the University Grenoble INP - Phelma, at the end of my international mobility period through the Erasmus+ programme, was based on a small part of a European project. In particular, the aim of the so called SiComb project is to develop an ultra-broadband frequency comb on a chip made of SiC, exploiting its unique optical properties such as the wide band gap.

In my case, the work involved depositing in an innovative way, i.e. at a low temperature (less than 800°C), a thin film of amorphous-SiC on top of a silicon wafer with a 2 µm silicon oxide layer on the surface and then carrying out heat treatments in order to obtain a recrystallisation of the silicon carbide layer itself. The purpose of this operation is to optimise the deposition and subsequent recrystallisation phenomenon in order to obtain a wafer with a silicon carbide thin layer on the surface through a relatively less expensive process, which could be the first step towards the realisation of these innovative optoelectronic devices.

Internship context

The internship was based on a little part of the European project called SiComb which have the aim to explore a new material platform, silicon carbide (SiC), which thanks to the unique optical properties of SiC (wide bandgap, high second-order and third order optical nonlinearity), is going to open the way to new optical devices including microcombs. SiC material is abundant and processing is complementary metal-oxide-silicon (CMOS) compatible. Thanks to the wide bandgap, the SiC frequency comb light source will cover ultra-wideband from near ultraviolet to middle infrared where disinfection, lighting, communication, biosensing and gas sensing have individual footprint, some of which is not covered by the standard lasers yet.

The high second-order and third-order nonlinearity of SiC makes the SiC frequency comb energy efficient. A frequency comb could replace thousands of standard lasers in the wavelength division multiplexing (WDM) technology of optical communications. These new SiC - based optical devices will also have important impact on quantum optics and quantum networks, quantum computing, sensing, and imaging, etc. A more secure and scalable integrated quantum networks based on these SiC optical chips are expected.

Moreover, new embedded biosensors based on compact SiC optical chips may revolutionize the current way of medical diagnosis because of the biocompatibility of SiC material.

Specifically, in datacentre networks, the new SiC material platform addresses squarely the current challenges. Amidst soaring demand for new services, industry seeks to double the bandwidth of datacentre switches every two years in order to keep pace with double-digit traffic growth. Indeed, optical technologies are striving to match the cadence of silicon evolution and, for the first time, optical I/O has a conspicuous position in the critical path of switch manufacturers in view of their next generation products. So, in prospective SiC optical chips will have wide and high impact in various field thanks to its unique optical properties as well as thermal, electronic, and mechanic properties. Despite the profound potential impact of SiC optical chips, there are also huge challenges to overcome, including tight optical confinement of the SiC waveguide nanostructures, low linear and nonlinear optical loss of the SiC waveguides, high quality factor of resonance cavity, phase control and stability of frequency comb. A number of developments have now made it relevant to demonstrate an on-chip SiC frequency comb (multiple lasers), a novel and challenging idea, because of the following crucial technology development: a) the SiC crystal quality has improved by the pull of SiC power electronics; b) Thin film transfer technology from a bulk

material, such as smart-cut method, has been developed; c) SiC surface polish technology is finely tuned; and d) there is a fundamental understanding of frequency comb generation and stabilization. These underlying technologies have laid a solid foundation for this proposal.

A CMOS compatible and ultra-broadband SiC frequency comb substantially outperforms other technological paradigms that currently exist or are under development. First of all, SiC is CMOS compatible, which outperforms InGaAs, AlN, and LiNbO₃ frequency combs. Secondly, SiC has wide bandgap (2.4-3.2 eV), which means a wide low-loss transmission window (400nm-5000nm) where the frequency comb could work. It also means very low two-photon absorption at the telecommunication wavelengths, which is crucial to reveal four wave mixing based nonlinearities. In this way, SiC microcombs are much broader in frequency and applications than Si and InGaAs combs, Thirdly, SiC possesses both high second-order and third-order optical nonlinearity. High third-order nonlinearity indicates it is promising to realize nonlinear effect-based supercontinuum or optical frequency comb. High second-order nonlinearity by itself could generate frequency comb and it could also wavelength convert the Kerr comb and extend the comb from infrared to visible for example. In contrast, amorphous material such as SiO₂, SiN or Hydrex normally does not have second-order nonlinearity. Si does not own second-order nonlinearity either because of the structural symmetry. Fourthly, SiC is bio-compatible. This is unique in all the materials mentioned earlier, which opens new potentials in biomedical applications. Fifthly SiC has very good thermal conductivity, and its thermal conductive coefficient is 3 times higher than Si; Last but not least, SiC is the second hardest material and very robust mechanically. Inspired by all these advantages of SiC, a nonlinear based SiC on-chip frequency comb will provide a solution to the most challenging research topics, including a CMOS compatible light source on photonic integrated circuits (PIC).

SiC has only one disadvantage at this stage: high cost. Thanks to the progress in diodes and MOSFETs for electronics and power devices, which have reached a commercial maturity in recent years, the volume production has created a profound drop of substrate cost. It is expected that further market entries, such as the new photonic devices and system applications to be achieved in this project, will drop the SiC prices even more. Un-matching the superior material properties of SiC, unfortunately, there is no world-wide research effort put in the SiC frequency comb yet. Despite the ground-breaking nature, SiComb also faces fierce challenges because SiC thin films are not well known in optics.

Internship work and objective

As just described in the previous paragraphs, the internship was based on a part of a European project (EU-funded SiComb) which aims to demonstrate for the first time a CMOS-compatible and ultra-broadband on-chip frequency comb made from sustainable and high-performance silicon carbide. SiMaP will try to develop high optical quality SiC thin films, i.e. with low optical losses. This requires a perfect control of both the bulk properties (volume) and the interface properties (layer/substrate interface and layer surface). These SiC thin films are deposited from the vapour phase at low temperature (typically lower than 800°C) on a silicon wafer covered by a SiO₂ layer on the surface. The silicon carbide layer consists in an amorphous phase due to the low deposition temperature, but upon specific heat treatments it could be recrystallized.

In particular, two deposition techniques have been exploited such as the PECVD and the sputtering PVD.

The objective of the internship is to study the behaviour of the as deposited films and after the annealing step, by a combination of in-situ and ex-situ characterization techniques such as the Raman spectroscopy, Ellipsometry, XPS and XRD. In this way, by depositing at such a low temperature a thin layer of SiC and then recrystallizing it, one could have a significant lowering of the production costs of this innovative material for new devices. Obviously, all this should be accompanied by a good quality in terms of properties of the layer itself after the heat treatment of recrystallization.

Chapter 1: Deposition methods

The relevance of thin films in the last decades has become increasingly important due to the constant demand from various technological fields such as electronics and the development of protective and/or functional coatings for specific applications.

The thin layer properties depend strongly on both the materials chosen and the deposition process. Consequently, the continuous research in this fields has necessarily led to a considerable development of the deposition techniques for the application of different materials on a variety of substrates, ensuring optimal quality. In general, a deposition accuracy of a few nanometres is achievable, but in specific cases, such as the atomic layer deposition (ALD) and the molecular beam epitaxy (MBE), it is even possible to deposit a single atomic/molecular layer at a time.

Thin film deposition techniques can be divided into two broad macro-categories, depending on whether the process is primarily chemical or physical. Chemical vapour deposition (CVD) is implemented through the chemical reaction of gas precursors at high temperature which allows the material, so the main product of the chemical reaction, to be deposited on a substrate, which also acts as a catalyst; this process is based on convective-conductive mass transport using an inert gas as carrier. The main problems of CVD are the deposition rate, the purity of the thin film and the generation of reaction by-products, which are generally dangerous and/or toxic.

Differently, physical vapour deposition (PVD) is obtained through the condensation of an evaporated material in vacuum providing a very clean process with a higher deposition rate. However, PVD is characterised by a less conformal deposition of the substrate surface structure and is not suitable for some materials due to the too high evaporation temperature. Within these two families, there are different deposition techniques depending on the pressures involved as atmospheric pressure (APCVD), low pressure (LPCVD) and very low pressure (VLPCVD), the presence of a plasma to increase the reactivity of the gases (Plasma Enhanced CVD), or depending on the method used for evaporation in PVD (thermal evaporation, ion beam and sputtering).

Since in our case the deposition have been carried out by PECVD and sputtering PVD, these two techniques will be described and analysed in the next paragraphs, so as to have a clear idea of how it works and what the main theoretical aspects underlying the process are.

1.1 Plasma Enhanced CVD – PECVD

The traditional CVD technique, as described above, is based on activating chemical reactions through thermal energy, so deposition temperatures are typically high. By exploiting the application of a plasma, a technique has been developed to be able to activate chemical reactions and carry out deposition at a lower temperature. This technique, called plasma-enhanced CVD (PECVD) or plasma-assisted CVD (PACVD), could be seen as the bridge between CVD and PVD techniques, as it combines a chemical and a physical process.

PECVD permits the coating of low-temperature substrates, favours the formation of amorphous or very fine-grained polycrystalline deposits and reduces the stresses caused by the thermal expansion mismatch between the substrate and coating. Moreover, the deposition rate is usually increased.

Plasma generation is achieved by applying an electric field (electrical energy) to a fixed quantity of gas: the molecules are dissociated into atoms, which in turn become ionised as they lose electrons. the plasma therefore consists of positively charged ions, electrons and possibly non-ionised atoms with a neutral charge (zero). However, if the electrical energy supplied is sufficiently high, it is possible to achieve complete dissociation, and thus complete ionisation.

Table 1 shows the main characteristics of the two different types of plasma used in CVD, glow-discharge plasma (non-isothermal) and arc plasma (isothermal). In particular, the first type will be described in more detail as it has been the one used for our SiC layer deposition (RF-PECVD).

	Glow-Discharge	Arc
Plasma Type	Non-Isothermal (non-equilibrium)	Isothermal (equilibrium)
Frequency	3.45 MHz and 2.45 GHz (microwave)	≈ 1 MHz
Power	1–100 kW	1–20 MW
Flow rate	mg/sec	none
Electron concentration	10^9 – 10^{12} /cm ³	10^{14} /cm ³
Pressure	200 Pa–0.15 atm	0.15–1 atm
Electron temperature	10^4 K	10^4 K
Atom temperature	500 K	10^4 K

Table 1: Characteristics of two different plasmas used in CVD systems [26].

The glow-discharge plasma is called non-isothermal because the electrons, which have an extremely small mass, are accelerated by the high-frequency electric field present and quickly reach high energy levels (corresponding to a very high temperature), while the ions

(which are much heavier) keep the plasma at a low temperature, not being able to follow rapid changes in field direction.

The high-energy electrons collide with the molecules of the gaseous precursors, resulting in dissociation and the generation of reactive chemical species and thus the start of the chemical reaction. Furthermore, since the pressure is low, the rate controlling is the surface kinetics which leads to a greater uniformity.

Microwaves (MW) at 2,45 GHz and radio frequency (RF) at 13,45 MHz (typical design in *Figure 1*) are the most common frequencies used in CVD.

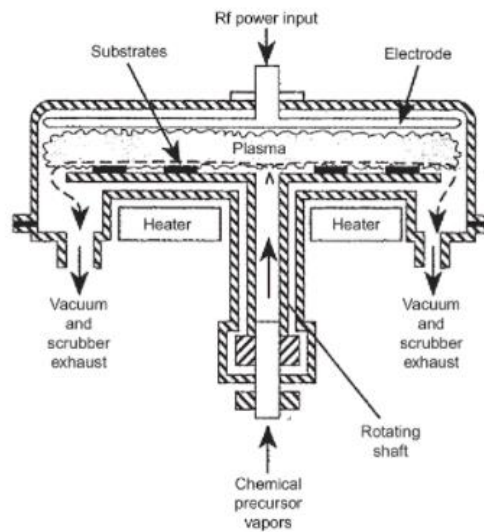


Figure 1: General design of a RF plasma CVD equipment [27].

To achieve a homogeneous and uniform deposition, the flow must be as laminar as possible. The basic parameters of the process are the concentration of the reactants, the temperature, the flow velocity and the thickness of the boundary layer, i.e. the layer of gas that actually reacts with the substrate. These parameters, together with the thermodynamic and kinetic aspects of the CVD process, will be described and analysed in the following paragraphs.

The limitations of PECVD are related to the difficulties in obtaining an exact stoichiometry and a high degree of purity of the deposited materials. Moreover, the equipment is generally more expensive and complicated.

1.1.1 Thermodynamics of CVD

A CVD reaction is governed by thermodynamics and by kinetics (it will be analysed in the next paragraph) which define respectively the "direction" and the "velocity" with which the chemical reaction is going to proceed.

The desired CVD reaction will take place if the thermodynamics is favourable, that is if the free energy change is negative, namely $\Delta G_r < 0$. To verify it, it is necessary to know the free energies of formation (Gibbs free energy, ΔG_f) of each compound [26].

$$\Delta G_r = \sum \Delta G_f \text{ products} - \sum \Delta G_f \text{ reactants}$$

The Gibbs free energy is not a fixed value, but it is influenced by the type and the molar ration of the reactants, and by the process pressure and temperature [26].

$$\Delta G_f = \Delta G_f^0 + RT \ln Q$$

where:

$$\Delta G_f^0 = \sum z_i \Delta G_{f,i}^0$$

z_i = stoichiometric coefficient of species “i” in the CVD reaction (negative for reactants, positive for products);

$\Delta G_{f,i}^0$ = standard free energy of formation of species “i” at temperature T and 1 atm;

R = gas constant;

T = absolute temperature;

$$Q = \prod_i a_i^{z_i}$$

a_i = activity of species “i” [$a_i = 1$ for pure solids and $a_i = p_i = x_i P_T$ for gases];

p_i = partial pressure of species “i”;

x_i = mole fraction of specie “i”;

P_T = total pressure;

Furthermore, the free energy change for a reaction at the equilibrium is zero by definition. The yield of a reaction is evaluated by calculating composition and activity (partial pressure for gases) in the equilibrium conditions.

Calculating the thermodynamic equilibrium (minimizing the Gibbs free energy) at constant temperature and volume, or at constant pressure, of a CVD system it is possible to have a better overview of the CVD reactions and a better prediction of the results. Indeed, it will provide useful information such as the optimum range of deposition conditions.

1.1.2 Kinetics and mass-transport mechanism

Once thermodynamic analysis has been done, it is necessary to study in depth the kinetic aspect. Indeed, to carry out the design and optimization of a CVD reactor it is important to

determine the reaction rate: this parameter is strongly influenced by the mass transport mechanism, that is how the reactants reach the deposition surface of the substrate.

It is important to specify that any CVD processes is characterised by a complicated fluid dynamic and, since a change of state from gaseous to solid occurs, by heterogeneous reactions. In particular, a gas flow made of a mix between precursors and transport gas enter in the reactor, diffuses through the boundary layer, and coming in contact with the substrate surface favours the deposition reactions. gaseous by-products are diffused away from the surface through the boundary layer (*Figure 2*). Basically, the slowest step of the sequence determines the deposition rate, and consequently the entire CVD process.

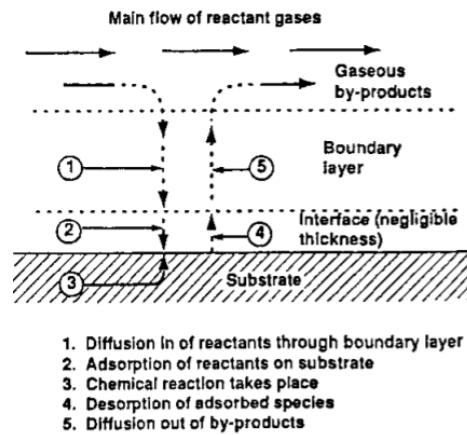


Figure 2: CVD sequence process during a general deposition [26].

As mentioned above, the gas flow should preferably be laminar in order to achieve a homogeneous and uniform deposition. In detail, the laminar flow is characterised by the fact that the gas velocity at the surface of the substrate is zero and gradually increases until it reaches the velocity of the bulk gas away from the substrate. This region of velocity variation is the boundary layer, mentioned several times previously.

The parameter that determines the type of flow of a fluid is the Reynolds number: roughly if $R_e < 2300$ the flow is laminar, if $R_e > 2900$ the flow is turbulent.

$$R_e = \frac{\rho u_x}{\mu}$$

Where:

ρ = mass flow density;

u = flow density;

μ = viscosity;

The boundary layer thickness is important because it is the gas portion that actually reacts with the substrate: a diffusion of the precursors flowing above this layer is involved to reach the deposition surface and guarantee the reactions.

The thickness of the boundary layer Δ is not everywhere constant, but decreases with higher gas-flow velocity and increases with moving away from the gas inlet tube x , according to the following equation [26]:

$$\Delta = \sqrt{\frac{x}{Re}}$$

However, far enough away from the gas inlet it tends to stabilise at a constant value as shown in *Figure 3*.

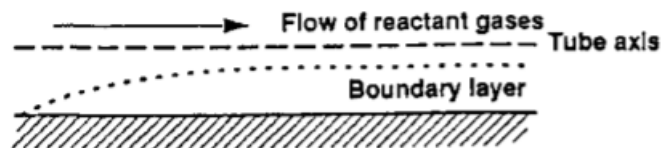


Figure 3: Boundary layer thickness evolution [26].

Further consideration to optimise the deposition reaction has to be done regarding the main factor which controls the growth rate of the deposit, called rate-limiting step. It is generally determined by either the surface reaction kinetics or by mass-transport, both influenced by temperature and pressure.

At low temperature and pressure, the control is referring to the surface-reaction kinetics: a considerable amount of reactants reach the substrate surface because the boundary layer is thin due to the high gas velocity and so the diffusion is facilitated. Conversely, at high T and P , the process is limited by mass-transport phenomena: in this case, the diffusion is more complicated because the gas velocity is low, resulting in a thick boundary layer.

So, briefly, in the first case the limiting factor is the availability of precursors on the surface and hence their concentration, while in the second case it is the diffusion rate through the boundary layer.

Clearly, at high temperatures the reaction rate will be higher and therefore the deposition is faster in the case of mass-transport control: once the system and the concentration of the gaseous precursors have been fixed, it is possible to optimise the thickness of the deposited film by suitably varying these two physical parameters.

1.2 Sputtering PVD

The sputtering PVD deposition process is a non-thermal vaporization technique where the vapour phase is obtained through a physical ejection of atoms from a target solid surface, with consequent deposition of these particles on a substrate. The mechanical ejection process is performed by momentum transfer from an atomic-sized energy bombarding particle, usually a gas phase (typically Ar), accelerated from a plasma: ion bombardment in a vacuum using an ion gun or low-pressure plasma (<5 mTorr), as in our case, to minimize the number of statistical collisions between sputtered particles and gas along the path target-substrate.

As in the case of CVD, there are different techniques for plasma generation: direct current (DC) is used for the deposition of conductive materials, while a radio-frequency configuration (RF at 13.56 MHz) is used for dielectric ones, in order to avoid a build-up of surface charge. A widespread variation of the process is the magnetron sputtering, which, using magnets, contains the plasma towards the target surface in order to optimise the system.

By blowing reactive gases together with Ar, it is possible to deposit materials from a reaction product onto the substrate, adjusting the stoichiometry according to the amount and speed of the incoming reactive gas: this process is called reactive sputtering PVD and increases the variety of materials that can be deposited.

In general, the sputtering PVD process (*Figure 4*) is characterised by a lower distance target-substrate and deposition rate but provides greater control over the thickness of the deposited film, also ensuring better uniformity in terms of topographical coverage of the substrate surface.

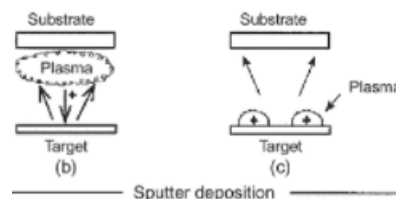


Figure 4: General sputtering PVD system [27].

An important parameter of this process is the sputtering yields, that is the ration between the sputtered atoms and the number of high energy incident particles, which depends on several factors: the mass, the energy and the angle-of incidence of the bombarding ions (*Figure 5*), and the target material. Moreover, to start the sputtering physical process is required a minimum amount of energy (generally <25 eV), named “threshold energy”, and the sputtering yields is not rather sensitive to the temperature of the target.

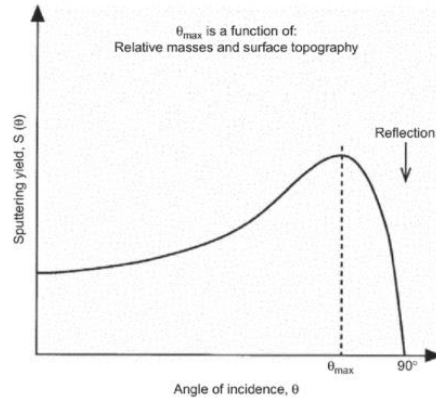


Figure 5: Sputtering yield as a function of the angle-of-incidence [27].

In particular, the energy transferred E_t by the physical collision can be expressed by the following equation [27]:

$$\frac{E_t}{E_i} = \frac{4M_t M_i (\cos \theta)^2}{(M_i + M_t)^2}$$

where:

E=energy;

M=mass;

i=incident particle;

t =target particle;

θ =angle of incidence;

The atoms, once they are vaporized from the sputtering target, must reach the substrate surface: in case of a sputtering PVD this distance is usually shorter compared to the traditional thermal evaporation, further limiting the interactions with the gas particles in the chamber. This energy-reduction phenomenon is called thermalisation and it is certainly influenced by the plasma pressure too.

As in the CVD process, temperature (together with pressure) plays a fundamental role in controlling the rate of deposition: at high temperatures, condensation on the surface of the substrate is promoted and accelerated by thermodynamic and kinetic effects.

Chapter 2: Characterization methods

Characterization methods are a fundamental step in materials science defined as the broad and general processes by which material's structure or properties are determined in a define and reproducible way. The techniques used may relate to the study of the structure and microscopic properties of the material, for instance microscopy and spectroscopy, as well as to macroscopic ones such as mechanical tests, thermal and optical analysis, etc.

Microscopy is the technical field of using different analysis equipment to probe and map the surface and sub-surface material structure, gathering data using photons, electrons, ions or cantilever probes. Common examples of these techniques are the optical microscopy, the scanning or transmission electron microscopy (SEM, TEM) and the scanning probe microscopy (SPM), subdivided in atomic force and scanning tunnelling microscopy (AFM, STM).

Differently, belong to the spectroscopy techniques all those characterization techniques which exploit physical and chemical principles to reveal the chemical composition, crystal structure and photoelectric properties of the materials using, for example, optical and X-ray radiation, such as Fourier transform infrared spectroscopy (FTIR), Raman spectroscopy, X-ray diffraction (XRD), energy or wavelength dispersive X-ray spectroscopy (EDX/EDS, WDX/WDS), Auger electron spectroscopy (AES) and X-ray photoelectron spectroscopy (XPS).

The characterization methodology, being often a comparative manner, should be more precise as possible, while accuracy depends on the type of measurement and the tool-equipment itself.

Typically, the characterisation of materials needed very sophisticated and costly instruments and requires a deep knowledge of the atomic and molecular nature of matter and the interaction between the probing species and atoms/molecules.

In the following paragraphs, the characterization methods mainly used in our case during the experimental work will be analysed in detail, namely Raman spectroscopy, XPS and XRD. Moreover, there will also be a subsequent section based on ellipsometry, as our field of application is optoelectronics, so the optical properties and thickness of the deposited film are crucial.

2.1 X-ray photoelectron spectroscopy – XPS

X-ray photoelectron spectroscopy is a surface-sensitive quantitative technique that identify the superficial chemical composition, and the chemical nature and state of the detected elements (electronic structure and density) exploiting the photoelectric effect. It analyses the energy of photoelectrons emitted from an X-ray bombarded surface in a vacuum environment. The vacuum level is very high, between 10^{-8} - 10^{-10} mbar, because the atmosphere in the chamber has not influence the surface composition/contamination and avoid multiple energy losses of the photoelectron due to the collisions during the path to reach the detector.

When an atom is invested by a photon, it absorbs and gains an energy amount equal to $h\nu$: to return to its stable energy state, it then emits an electron with a kinetic energy to the difference between the photon incident energy and its binding energy (*Figure 6*). In reality, there is a further energy component, a standard value called surface energy, which takes into account the energy required to cross the surface.

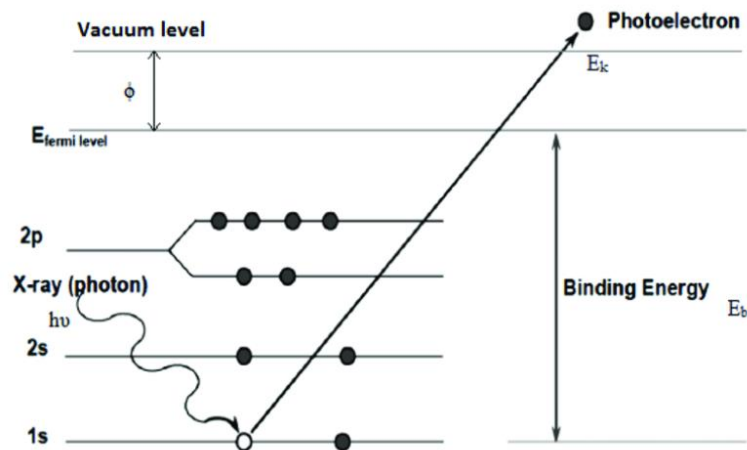


Figure 6: Diagram of a generic photoelectric effect in XPS [28].

Thus, XPS measurement depend on the energy of the X-ray used and usually a monochromatic beam is used to have an improved resolution, but sometimes it can be also non-monochromatic. In particular, K_α X-ray radiation from Mg (1253.6 eV) or Al (1486.6 eV), as in our case, are the most common sources exploited for this analysis. A slightly modification of the Beer's law can explain the photoemission intensity from an overlayer (O) and for the substrate (S) covered by an overlayer. In particular, the XPS results is obtained by subtracting these two following equations, to have a clear analysis of the surface:

$$I_{k_o} = I_{o_o} [1 - e^{(-d/\lambda \cos \theta)}]$$

$$I_{k_s} = I_{0_s} [e^{(-d/\lambda \cos \theta)}]$$

where:

I_0 = incident intensity;

I_k = exiting photoelectron intensity;

d = thickness of the overlayer;

λ = inelastic mean free path (absorption coefficient);

θ = angle of incidence;

The angle of incidence and the inelastic mean free path (distance between two different inelastic collisions) also influence the depth of analysis y , which can be expressed according to:

$$y = 3\lambda \sin \theta$$

Usually the value of y at 90° is about 10 nm, while the spot size ranges from 10 μm to 200 μm .

Therefore, measuring the velocity of the photoelectron emitted by a cylindrical mirror analyser, it is possible to calculate the energy binding which is referred to its chemical environment in the material.

$$E_b = E_{ph} - E_k - E_{surf}$$

After the emission process, the atom can reorganise its electron-energy structure by dropping an electron from a higher energy level to a vacant core hole: the excess of energy can be ridded by ejecting a second electron from a higher energy level, called Auger electron, or by emitting an X-ray photon through the X-ray fluorescence process. The presence of high-energy electrons related to the Auger effect must therefore also be considered in the measurement spectrum, and it is possible to differentiated from the photoelectrons because they have characteristic energy that does not depend on the energy of the incident radiation.

A general scheme of a XPS device is reported in *Figure 7*.

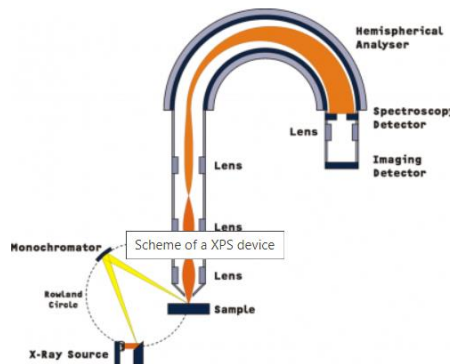


Figure 7: General scheme of a XPS device [29].

The energy binding is correlate to the chemical bonding between atoms in the material and important information can be obtained from the “chemical shift” of the XPS electron energy position. Changing the electric potential in the hemispherical analyser it is possible to change the trajectory of the photoelectrons to select and study a single element spectrum, improving the resolution of the measurement respect to the general survey one.

2.2 Raman spectroscopy

Raman spectroscopy is one of the most important vibrational spectroscopies which provide a chemical and structural fingerprint of materials through the analysis of characteristic fundamental vibrations mode. This technique involves the study of the interaction of radiation with molecular vibration: it is a two-photons inelastic light scattering event. A sample is invested by photons using a laser beam (visible, n-IR, n-UV); the incident photons have higher energy than the vibrational quantum energy and lose part of their energy due to the interaction with the molecular vibration, subsequently diffusing at a lower frequency. The Raman spectroscopy typically refers to the use of laser wavelengths which are not absorbed by the sample.

A general scheme of a Raman spectroscopy device is reported in *Figure 8*.

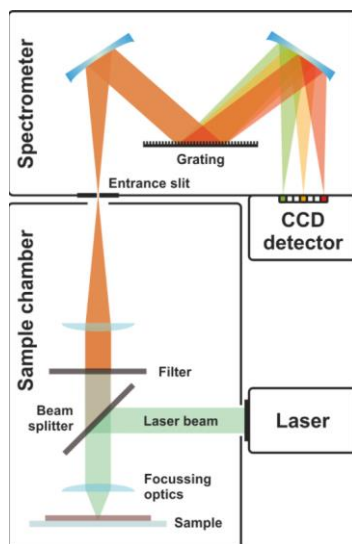


Figure 8: General scheme of a XPS device [30].

Therefore, Raman shift is characteristic of each different vibrational mode of the molecules and it is typically reported in wavenumbers, which has units of inverse length: expressing the wavelengths in nm gives the Raman shift in cm^{-1} according to this formula:

$$\Delta\tilde{\nu} (\text{cm}^{-1}) = 10^7 \left(\frac{1}{\lambda_0} - \frac{1}{\lambda_1} \right)$$

The frequencies of the molecular vibrations, indeed, depend on the masses of the atoms, the chemical bond strength and their geometric arrangement.

A rough subdivision of the vibrational spectrum into typical regions can be the following [30]:

- X-H stretch highest frequencies (3700-2500 cm^{-1})
- $\text{X}\equiv\text{Y}$ stretch and cumulated double bonds $\text{X}=\text{Y}=\text{Z}$ asymmetric stretch (2500-2000 cm^{-1})
- $\text{X}=\text{Y}$ stretch (200-1500 cm^{-1})
- X-H deformation (1500-1000 cm^{-1})
- X-Y stretch (1300-600 cm^{-1})

In the real scenario, the actual vibrations of molecules often involve coupled vibrations.

2.3 X-ray diffraction – XRD

X-ray diffraction is one of the different diffraction methods which are generally used to determine the crystal plane spacing, the crystallographic phase composition, preferential orientation of the structure, grain size and lattice distortion. This technique exploits the Bragg's law irradiating a substrate film with a short-wavelength X-rays.

$$n\lambda = 2d \sin \theta$$

where:

n = diffraction order;

λ = wavelength;

θ = exit radiation angle (glancing angle);

d = interplanar distance (grating constant);

A monochromatic X-ray beam is generated, by a cathode ray tube, and focus on the sample surface to produce a constructive interference through the X-ray-sample interaction (*Figure 9*).

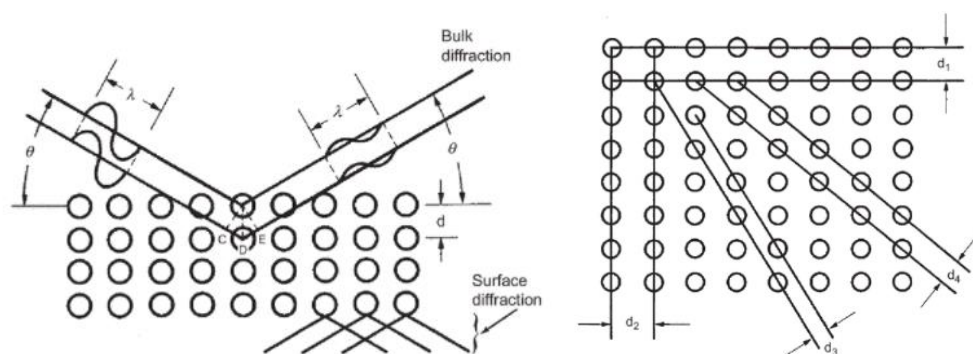


Figure 9: Diffraction of radiation and interplanar spacing and plane population [27].

The crystal, placed under an intense X-ray beam, is scanned by gradually rotating it as the measurement proceeds. Taking into account that each compound has a unique diffraction pattern, the angles and intensities of the diffracted X-rays are measured. As the rotation takes place, previous reflections disappear and new ones appear; the intensity of each point is recorded at each orientation of the specimen. By comparing the diffraction patterns as a function of 2θ angle obtained from standard reference measurements, it is possible to correlate the different materials to the different crystal phases.

It is important to notify that slight differences between two measurements of the same crystal phase are possible, and they are related to variation of cell parameters, due to internal stresses for instance, amount of crystalline phase (variation of the integrated area of a peak), crystallite size, presence of defects, etc.

2.4 Ellipsometry

Among different optical techniques there is the ellipsometry which analyses the dielectric properties, such as refractive index or dielectric function tensor, of a thin film using an incident radiation: it measures the polarization change upon reflection (or transmission) and compares it to standard models.

The polarization change is quantified by the amplitude ratio Ψ and the phase difference Δ : these two factors can parametrise the complex reflectance ratio ρ , result of an ellipsometry measurement [31]. In particular, ρ is the ratio between the amplitudes of the component which oscillates parallel to the incidence plane p and the perpendicular oscillating component s , after the reflection step and the normalization to their initial value (respectively r_p and r_s).

$$\rho = \frac{r_p}{r_s} = \tan \Psi \cdot e^{i\Delta}$$

To ensure a maximal difference between r_p and r_s , so to have a consistent measurement, the angle of incidence is chosen close to the Brewster's angle θ_B of the sample [32]. Moreover, since this measurement is a ratio of two values, it has a high degree of reproducibility and accuracy.

$$\theta_B = \tan^{-1}\left(\frac{n_2}{n_1}\right)$$

where:

n_1 = refractive index of the initial medium;

n_2 = refractive index of the second medium;

The ellipsometry is very sensitive to the characterization of thickness, composition, crystalline nature, surface roughness, electrical conductivity, and doping concentration. A general scheme of a Ellipsometry device is reported in *Figure 10*.

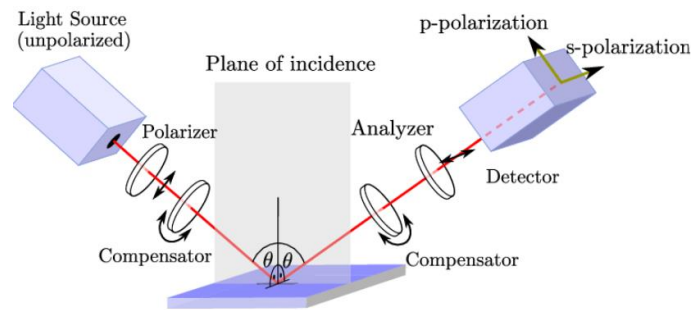


Figure 10: General scheme of a XPS device [33].

Chapter 3: Experimental work

To carry out the purpose of the internship, a silicon carbide layer has been deposited through two different techniques as the PECVD and PVD, with a thickness goal of about 500 nm to have a low optical loss component. The starting wafers used were 4-inch silicon wafer with a thickness between 500-550 μm on which a silica layer of about 2 μm was grown by heat treatment oxidation.

On the wafer 1 the PECVD deposition of the SiC layer has been performed by a French company (Corial) using their own equipment characterized by a uniformly heated pressurized reactor design for high uniformity of thickness and deposited film properties. In the *Table 2* are reported the deposition parameters used for the PECVD.

PECVD	
Temperature	300°C
Precursor gas	C ₂ H ₄
Gas flow rate	131 sccm
Deposition rate	142 nm/min

Table 2: PECVD deposition parameters.

Since the PVD deposition has been accomplished in the SiMaP laboratory, the silicon carbide thin layer has been made by two different deposition parameters “A” and “B”, listed in the *Table 3*, respectively used for the wafer 2 and 3.

PVD	Deposition “A”	Deposition “B”
Temperature substrate	500°C	750°C
Plasma pressure	0,5 Pa	0,1 Pa
Chamber pressure	10 ⁻⁶ mbar	10 ⁻⁶ mbar
Deposition time	120 min	90 min
Argon flow rate	40 sccm	40 sccm
Power	300 W	300 W

Table 3: Different deposition parameters used in the PVD.

After the deposition process the three wafers have been cut in small squares (15x15 mm) to allow the different characterisations and heat treatment experiments; since the purpose on the internship was to analyse the behaviour of the layer at high temperature, verifying the

possibility to recrystallize the amorphous layer deposited, many different heat treatments have been done, described later in the chapter *Heat Treatments (Annealing)*.

To characterize the films deposited before and after the various heat treatments, several techniques and measuring instruments have been used. An optical microscope to analyse the surface of the samples; ellipsometry to assess the thickness and optical properties; X-Ray photoelectron spectroscopy (XPS), Raman spectroscopy and X-Ray diffraction (XRD) to perform a chemical and structural analysis (before and after the annealing processes) and verify the onset of the recrystallization phenomenon.

3.1 Layer characterisation – as deposited

In this section all the results, coming from the characterisations of the SiC layers as deposited, have been reported. It has been analysed one sample (small square) of each wafer using three different measurements: the ellipsometry to measure the thickness and the optical properties, and the Raman and the X-ray Photoelectron spectroscopies to have a chemical and structural analysis of the films.

3.1.1 Ellipsometry measurements

It has been used an ellipsometer to measure the deposited layer thickness and its optical properties as the refractive index and the extinction coefficient (n and k factors). To have a good fit of the optical curve measured has been necessary utilise two different fitting laws as appropriate: the Tauc Lorentz or the Cody Lorentz law. Basically, the difference between the two laws is not very important because is referred only at the high energy absorbance property which is not very relevant for the purpose and the goal of the internship. It has not been found a clear reason explanation of this not congruent aspect.

In *Figure 11* are reported the two property curves varying the wavelength of the PECVD sample and the *Figure 12* and *Figure 13* show respectively the refractive index and extinction coefficient of the PVD samples.

Analysing the property curves for all the samples the main trend has been found decreasing with the wavelength, as expected; a different trend can be seen at low wavelengths, therefore at high energies, in which the refractive index of the wafer 1 (PECVD deposited) and the extinction coefficient of the wafer 3 have a different trend. Anyway, to have a clear comparison between the different samples and with the values in literature about the refractive index and the k parameter, it has been chosen to utilize the values obtained at the

wavelength of 677 nm. In particular, it has been found a value of $n=2.65$ for the SiC crystalline which it will be used to compare the different sample, even if the deposited layer in our case is amorphous.

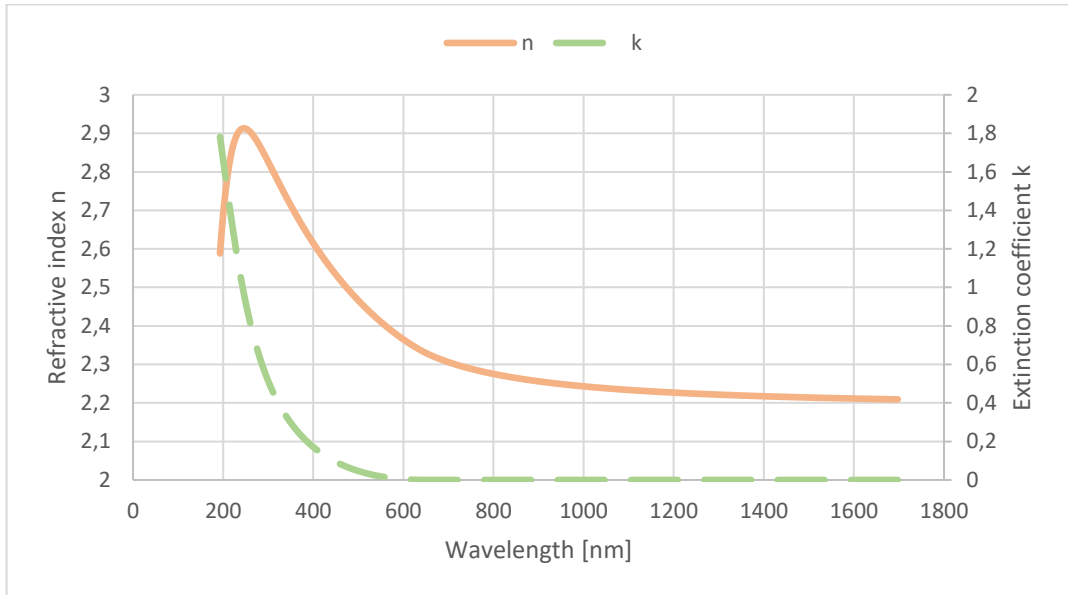


Figure 11: optical properties n and k of the PECVD samples.

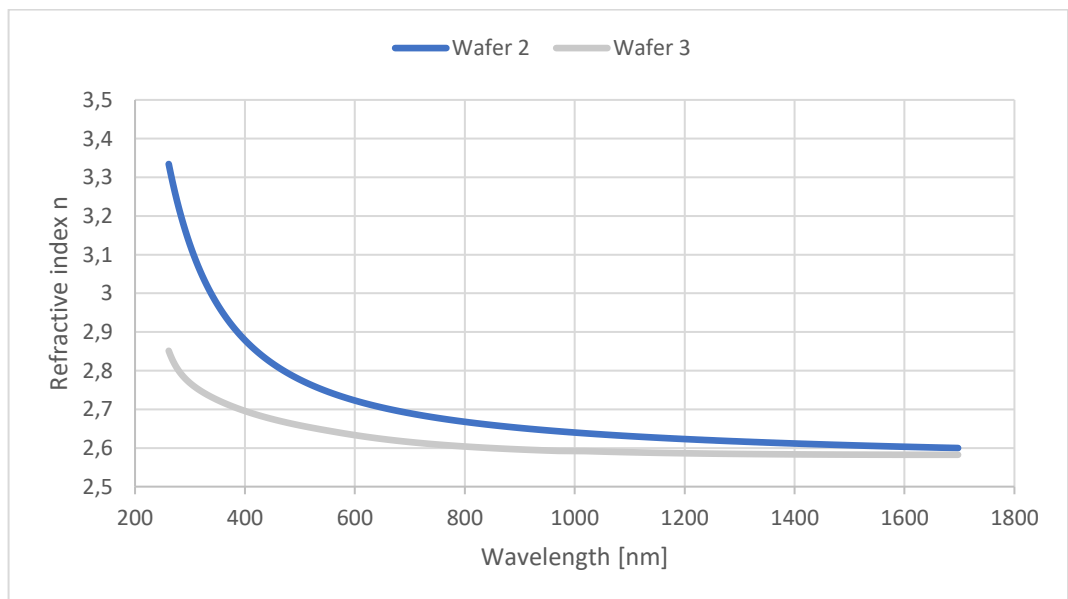


Figure 12: Refractive index in function of the wavelength for the PVD samples.

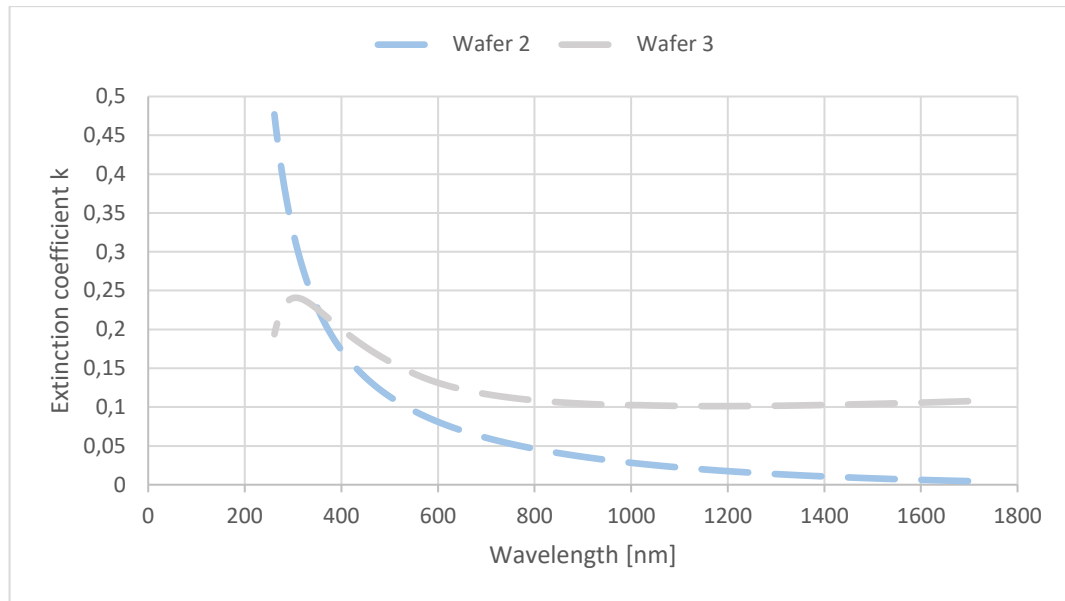


Figure 13: Extinction coefficient in function of the wavelength for the PVD samples.

The *Table 4* shows some resume output data from the measurements as the fitting law used, the layer thickness of the film, the value of surface roughness and the n and k values at fixed wavelength. In this way it is possible to have a clear and simple comparison between all the three different samples.

First of all, the deposited thickness was not perfectly 500 nm, but it was lower for PECVD deposition (about 350 nm) and higher for PVD (about 600 nm). However, this is a problem that can be solved adjusting the deposition parameters (the deposition time for example) carrying out various experiments and looking for the optimal ones. Anyway, this difference in thickness will not influence the final internship purpose because it was just a starting idea and it will not affect the experimental data.

The n and k values measured on the PVD wafers is clearly higher as compared to the PECVD one, probably due to the presence of the H; it is important to mention the fact that the requirement for the application of reference is to have the highest possible refractive index and the lowest possible extinction coefficient.

The reported value of the surface roughness is only qualitative as with the ellipsometry the surface quality is calculated through an optical measurement and it is obtained by simulating a surface layer composed partly of the real material and partly of air; the thickness obtained of the aforesaid layer indicates the surface roughness. It would be more appropriate to couple this type of result to a more specific measure, such as the AFM, to assess its accuracy and reliability. Therefore, throughout the treatment of the report, this value will be reported in

order to have a qualitative parameter and to be able to roughly compare the different values (when it has been possible to calculate it).

	Wafer 1	Wafer 2	Wafer 3
Deposition	PECVD	PVD - “A”	PVD - “B”
Fitting law	Tauc-Lorentz	Tauc-Lorentz	Cody-Lorentz
Layer thickness	347 nm	587 nm	604 nm
Surface roughness	6 nm	17 nm	27 nm
n@677 nm	2.32	2.70	2.62
k@677 nm	0	0.06	0.12

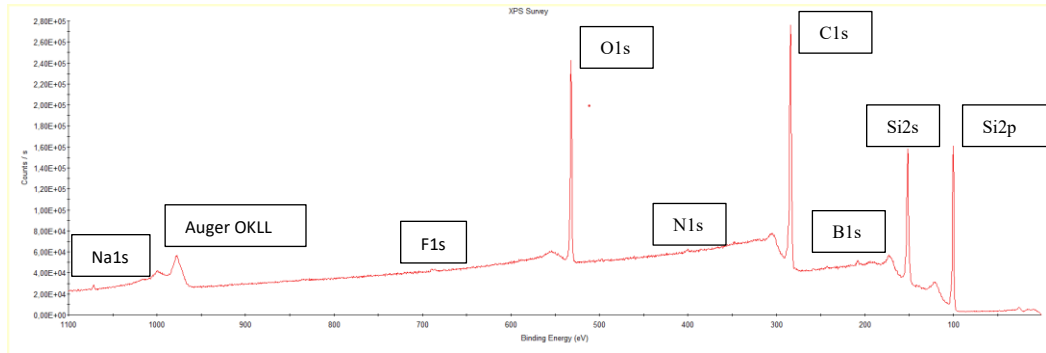
Table 4: Summary of the ellipsometry measurement's values for all the samples.

3.1.2 XPS analysis

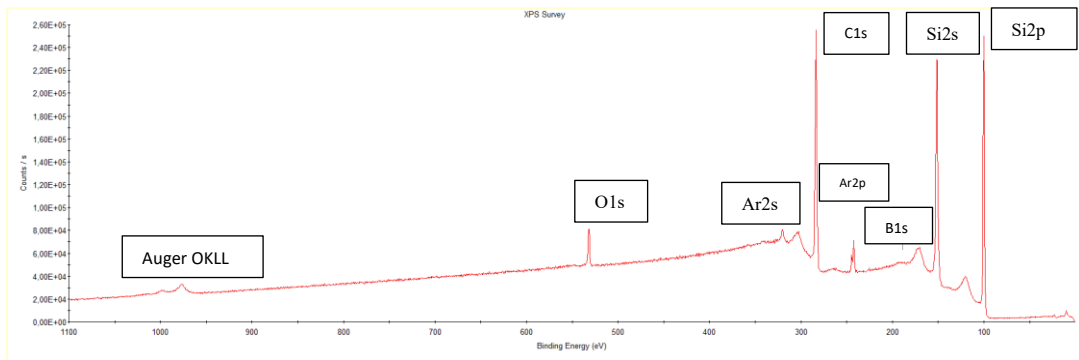
It has been exploited the XPS technique to study the chemical state and composition of the surface. For all the specimens (including those subsequently annealed, which will be described and discussed later) a general analysis on the surface (XPS Survey) has been carried out first and then, a specific analysis on the two elements mainly presents in the layer (in this case Si and C). In addition, these two measurements have been also performed after an Argon etching to be able to distinguish surface contamination from the real material.

Analysing the XPS Survey of the samples, before (*Figure 14a, 15a, 16a*) and after argon etching (*Figure 14b, 15b, 16b*), the eventual presence of Ca, Na, F and a high presence of oxygen can be traced back to a surface contamination as they always disappear, or decrease as the oxygen, after the erosion treatment; obviously, the presence of Ar in the “after etching” results is a result of the argon etching process itself. Instead, the traces of N and B in the PECVD sample, and the Cl, Ar (few traces coming from the plasma) in the PVD samples is a material contamination probably referred to the deposition process, because they are present also after the etching process. In our case, these contaminations are not very relevant as the amount is low and do not significantly affect the properties studied and the internship goal.

Anyway, it would be advisable to optimize the deposition processes also for this reason, in order to minimize surface contamination, and not only to control the thickness of the deposited layer.

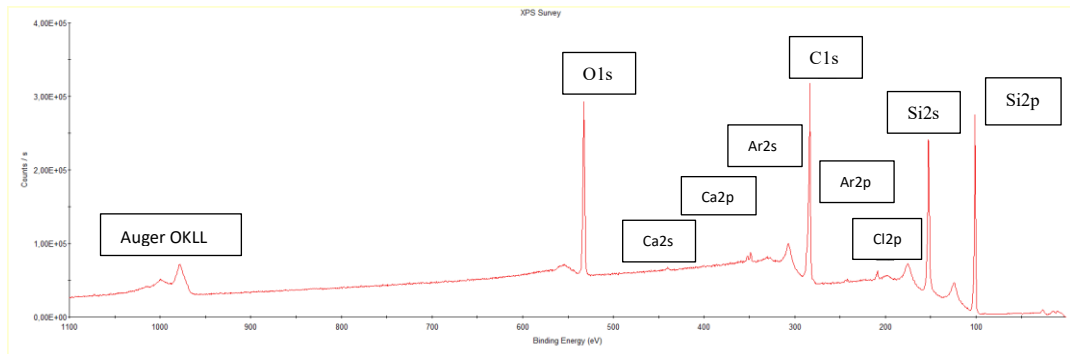


(a)

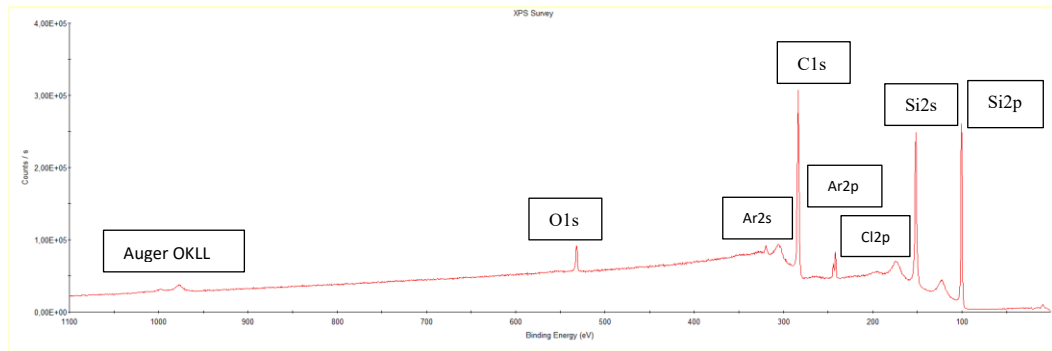


(b)

Figure 14: XPS survey of the PECVD sample before (a) and after (b) Ar etching.

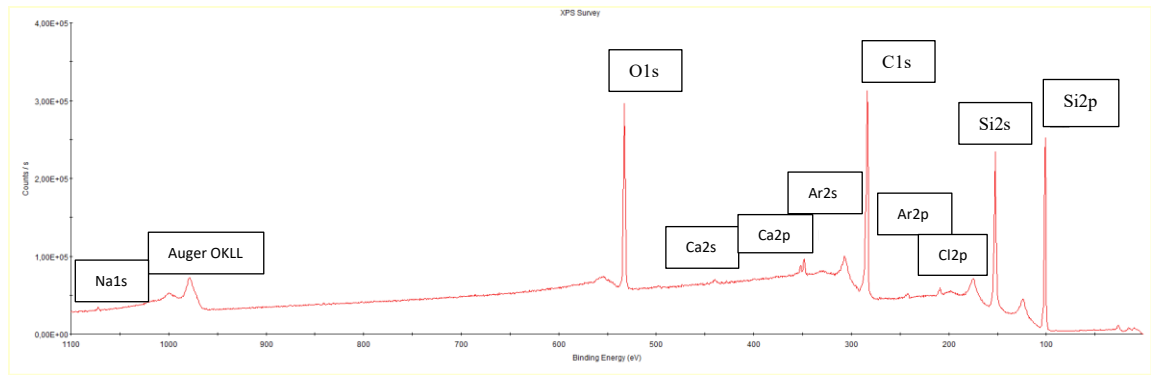


(a)

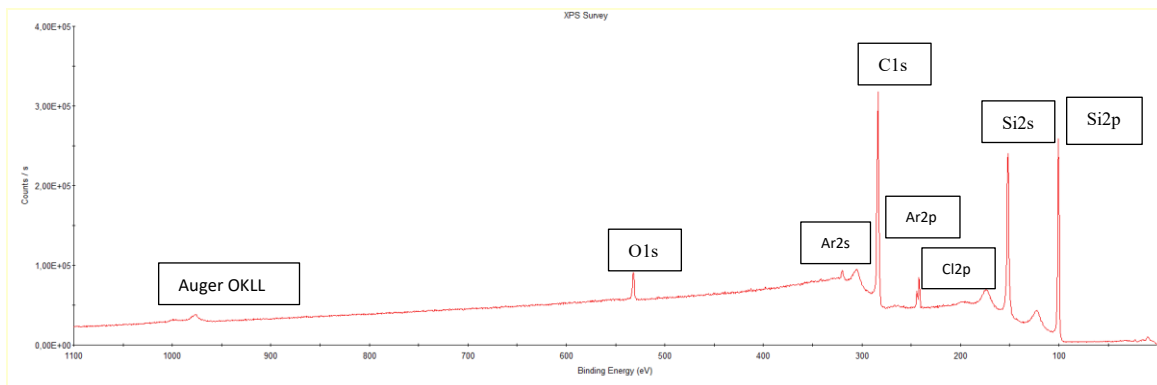


(b)

Figure 15: XPS survey of the wafer 2 before (a) and after (a) Ar etching.



(a)



(b)

Figure 16: XPS survey of the wafer 3 before (a) and after (b) Ar etching.

A more accurate analysis has been made on the silicon and carbon peaks in that they are the elements constituting the SiC layer studied: for all the samples the XPS spectra was investigated deeply in the 97-104 eV (Si 2p) and 280-287 eV (C 1s) regions. So, it is possible to study the various bonds of Si and C atoms, but it is necessary to have a referring table to couple the binding energy values to the chemical bonds themselves. As first approach it has been done an accurate literature review to have an initial overview of the binding energy of the principal bonds and then, since each experimental system and material could have its own nuances, it has been drawn up the *Table 5* and the *Table 6* containing the values of the bonds of the PECVD and PVD samples so that everything was congruent and logical. Obviously, the tables are just a first hypothesis that has to be verified and demonstrated by following experiments.

The yellow bonds are referred to the material without the surface contamination, that is, the values which indicate the SiC layer chemical structure itself.

In some case different bonds has been considered not discriminable and so they were grouped in a single binding energy value, not always in agreement with the literature. Regarding the C-Si and C-C bonds present in the layer, it has been developed the hypothesis

of a material composed not only by SiC, but with some areas in which the C is bonded with itself. This assumption has been taken into account for the PVD samples too.

PECVD		
C1s		
Chemical Bond	Binding Energy (eV)	FWHM (eV)
C-Si	283.1±0.2	1.6±0.1
C-C	284.2±0.1	1.5±0.2
C-H	285.4	1.7±0.1
C-O	286.3	1.7±0.1
C=O	288.4	1.6±0.1
Si2p		
Chemical Bond	Binding Energy (eV)	FWHM (eV)
SiC (/Si-Si/Si-H)	100.1±0.1	1.6±0.1
O-Si-C	102±0.1	1.5±0.1
SiO ₂	102.9	1.4

Table 5: Binding energy reference table for the PECVD sample, about Si and C.

PVD		
C1s		
Chemical Bond	Binding Energy (eV)	FWHM (eV)
[C ⁴⁺ single carbide species]	282.1±0.2	1.2±0.1
C-Si	283.2±0.2	1.1±0.2
C-C	284.2±0.2	1.7±0.1
C-H	285.4±0.2	1.5±0.3
C-O	286.4±0.2	1.5±0.3
Si2p		
Chemical Bond	Binding Energy (eV)	FWHM (eV)
SiC (/Si-Si) (before etching)	101.1±0.2	1.2±0.1
SiC (/Si-Si) (after etching)	100.6±0.1	1.6±0.1
O-Si-C	102±0.2	1.5±0.3
SiO ₂	103.4±0.2	1.6±0.1

Table 6: Binding energy reference table for the PVD samples, about Si and C.

The situation of the Si 2p is more complicated to analyse because besides the fact that the presence of H was not detectable for the PECVD layer (given the process itself, it is normal to find H within the layer) and there was no trace of the Si-Si bonds; if there are some areas of C, some Si has to be linked somewhere, so it is clear that the Si-Si (and Si-H too) bonds are hidden somehow. Moreover, the energy binding of the Si-C bonds was shifted to lower values respect to the literature in both cases, although more in PECVD than in PVD.

For these reasons it has been supposed that the Si-C, Si-Si and Si-H were not discriminable and able to shift the binding energy through lower values, so considered grouped in a single binding energy. Indeed, looking at the “after etching” values of the SiC binding energy groups, the PECVD sample has lower value than the PVD ones due to it has two “shift

components” inside (Si-Si and Si-H), while the seconds have just one added component in the group (Si-Si).

The experimental data from the XPS, wafer 1 and 2 are reported in the following pictures: *Figure 17* (PECVD sample after Ar etching) and *Figure 18* (PVD wafer 2 after Ar etching); all the results from the surface analysis before etching for what concern the specific result of Si and C bonds and from the wafer 3 are reported in the *Appendix*.

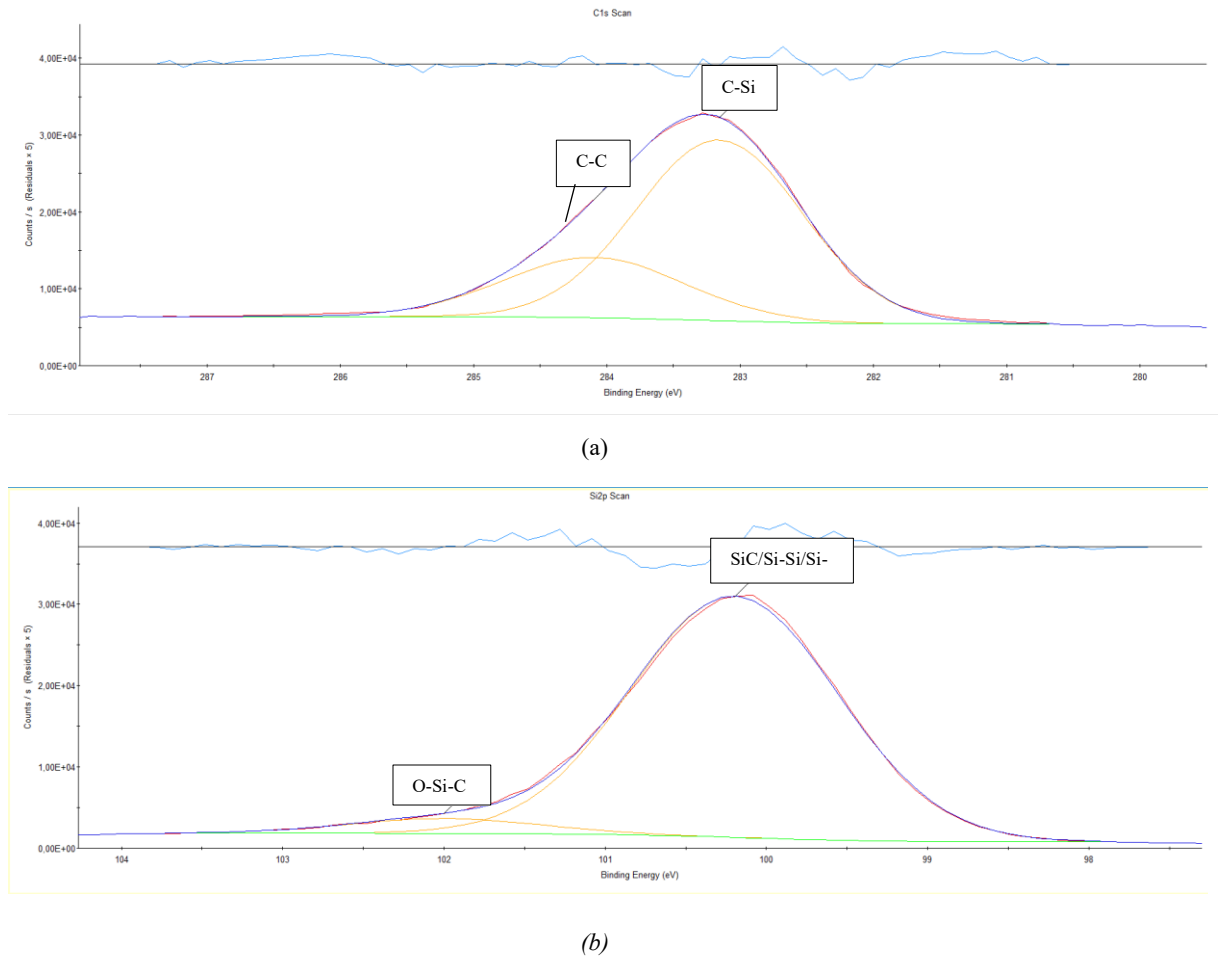
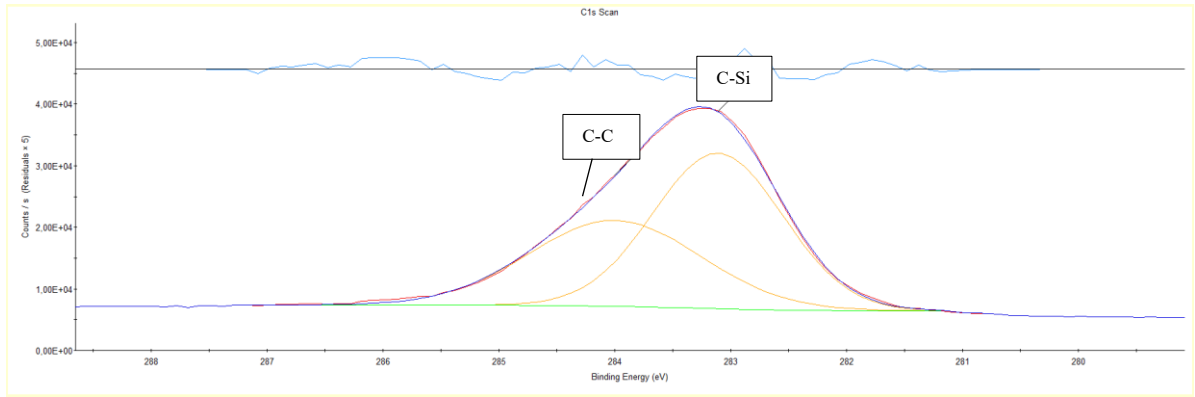
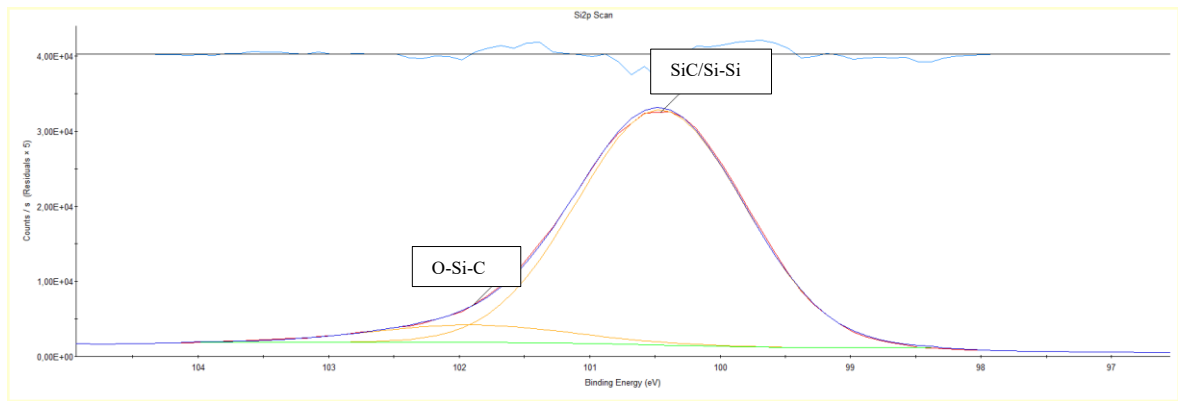


Figure 17: XPS results for C1s scan (a) and Si2p scan (b) from PECVD sample after etching.



(a)



(b)

Figure 18: XPS results for C1s scan (a) and Si2p scan (b) from the wafer 2 (PVD) after etching.

The measurements, also in this case, have been done both before and after etching to discriminate the surface contaminations from the material's layer itself (pictures in *Appendix* as already said). In the PECVD sample the impurities are constituted by the silicon oxide, C-OH, C-O and C=O, while for the PVD samples it is not present the C=O bonds. Moreover, it can be noticed that in the wafer 2 (and wafer 3) there is a little peak at the binding energy of about 282.1 eV which is possibly referable to the single carbide species (C^{4-}), as it has been suggested in the article but given the size it might not be an actual peak but part of the error between the fitting and the experimental measurement. Another important point to mention is that in these PVD samples, focusing the silicon spectra, there is a significant difference in the binding energy on the fundamental bonds of the material before and after etching (from about 101.1 eV to about 100.6 eV) probably due to the presence of the Ca as a surface contamination.

3.1.3 Raman spectroscopy analysis

It has been exploited the Raman spectroscopy measurement to have another point of view of the system, providing a structural fingerprint of the layer, so allowing a better understanding of the previous results. Indeed, it has been important to intersect the two different spectroscopies to build a solid and acceptable hypothesis on the layer's chemistry and structure.

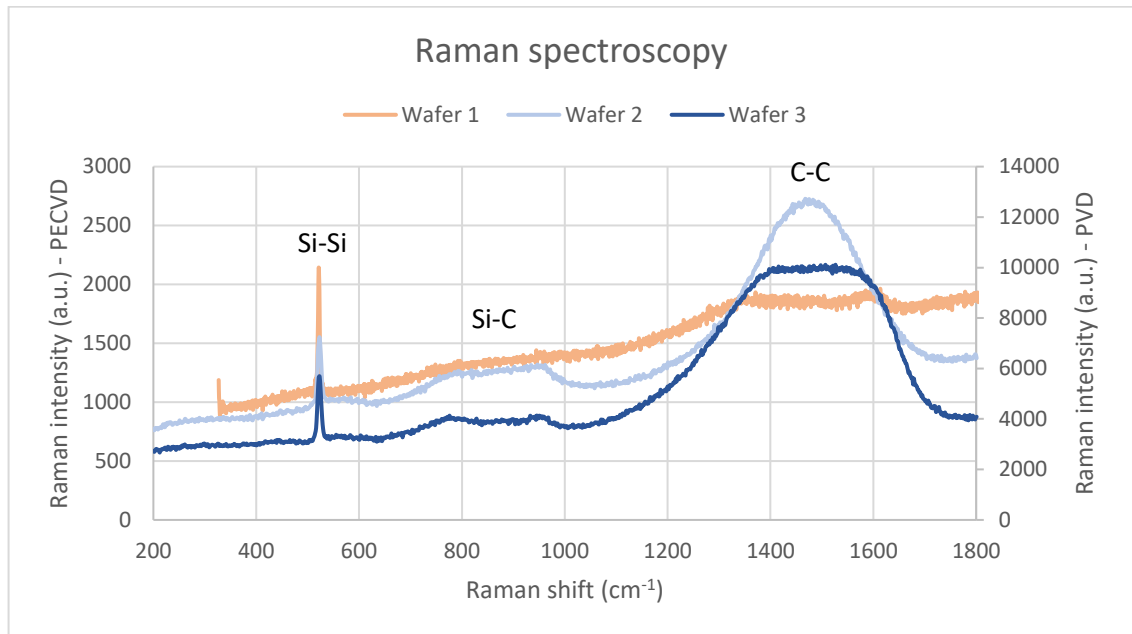


Figure 19: Raman spectroscopy for all the specimens as deposited.

The Figure 19 shows the Raman spectra in which, for all the samples, it is possible to notice clearly two different zones detected by the measure: a peak around 520 cm^{-1} attributable to the crystalline silicon (basically deriving from the substrate) and a broad peak around $1300\text{--}1650\text{ cm}^{-1}$ respective to the carbon area. The presence of such a large peak can be justified by the presence of the amorphous C inside the layer, confirming the XPS results with respect to the notable presence of C-C bonds. The different shape of this area in the three specimens is referred to the “very poor” graphitization of the carbon where it is visible a greater width of the area, so in the wafers 1 and 3.

However, the very particular thing concerns the scarce presence of a signal with a broad peak in the $780\text{--}970\text{ cm}^{-1}$ zone of the spectra (in the PECVD practically absent), which is inherent to the silicon carbide area. This result can be attributed to the fact that the layer in question is very thin, approximately between about 350 nm in one case and about 580 nm in the others: indeed, this zone is much more detectable in the PVD samples in with the

thickness of the SiC layer is higher than the PECVD one. Moreover, it is also possible to state that the silicon carbide predominantly present is not crystalline but amorphous; this fact will be demonstrated afterwards with the XRD measurement and in the evolution of the crystalline SiC on the XRD spectra before and after the heat treatments.

3.2 Heat treatments

To follow the internship purpose it has been necessary to conduct several heat treatments trying to recrystallize the amorphous SiC layer deposited on the three wafers. In particular, two different furnaces have been utilised depending on the final goal: a furnace capable of going to very high temperature to carry out a simple annealing at fixed temperature (with controlled atmosphere and $T > 1100^{\circ}\text{C}$), and a specific furnace (made-up by SiMaP laboratory) to have in-situ measurements and therefore greater control of the treatment itself (with controlled atmosphere and $T < 1200^{\circ}\text{C}$).

In situ measurements consist in continuously recording the value of the surface curvature of the specimen and the reflectance using three lasers with different wavelengths (405 nm, 633 nm, 949 nm); from the abrupt variation of the aforementioned properties, it is possible to identify the events that occurred during heating or cooling, which will subsequently be studied, analyzed and understood. The specimens to be used in this special furnace are 15x15 mm square in size.

Regarding the first furnace mentioned, a specific size is not required for the specimens, but the important thing is that they can fit inside the graphite container that is placed inside the furnace.

After each heat treatment carried out, the specimens were again analysed with the techniques already mentioned and described: ellipsometry, XPS, Raman spectroscopy. Moreover, an experimental measurement has been added to the XRD, in the case of the specimens in which the deposition took place via PVD, in order to detect the possible recrystallization of the SiC layer; this is because it cannot be detected with the previous techniques.

3.2.1 PECVD samples

In this section the treatments carried out on the samples deriving from the wafer 1 will be described and analysed; the *Table 7* is reported as a summary to visualise all the experiments done.

As can be seen, the first annealing performed at $T=1300^{\circ}\text{C}$ under vacuum for 1 hour led to the complete delamination of the deposited layer. In fact, although it was already clear to a simple visual analysis, this fact was immediately confirmed by the measurements derived from ellipsometry and XPS (reported in the *Appendix*); in both cases, only the $2\ \mu\text{m}$ silicon oxide layer on the starting wafer was detected.

PECVD	Temperature	Pressure	Atmosphere	Time	Note
Annealing 1	$T=1300^{\circ}\text{C}$	2 mbar	Vacuum	1 h	Delamination
Annealing 2	$T=1100^{\circ}\text{C}$	500 mbar	Argon	1 h	Delamination
In-situ measurement	Plateau at $T=770^{\circ}\text{C}$ Plateau at $T=1080^{\circ}\text{C}$	3 mbar	Argon	About 1 hour each plateau	Event at about 500°C in all the properties
Heat treatment	$T=450^{\circ}\text{C}$	Atmospheric	Air	About 6 h	Beginning of a delamination phenomenon

Table 7: Heat treatments summary for the PECVD samples.

Assuming that the problem could be a degradation phenomenon, a second annealing was performed at a lower temperature ($T=1100^{\circ}\text{C}$) and higher pressure (500 mbar) using Argon as a gas, for 1 hour as well. However, even in this case the complete delamination of the SiC layer occurred, excluding the possibility of the presence of a degradation reaction.

At this point it was decided to carry out a heat treatment in the specific furnace that would allow to make in situ measurements, in order to try to understand which the cause of delamination was. To verify the possible onset of some slow phenomenon, the temperature was stopped twice for about an hour: at $T=770^{\circ}\text{C}$ and at $T=1080^{\circ}\text{C}$. The whole experiment was conducted in an Argon atmosphere at about 3 mbar pressure.

As can be seen in *Figure 20*, at about 500°C there is an abrupt decrease in refractivity (for both the three wavelengths) and an uncontrolled increase in the surface temperature of the specimen (it does not follow the thermal ramp): the exposed layer is no longer silicon carbide but silica.

The same event has been recorded in the case of the curvature: at about 500°C there is a sudden decrease in the value of the curvature (*Figure 21*). It is important to point out that at the end of the second thermal plateau ($T=1080^{\circ}\text{C}$) there seems to be another event like the

previous one, however this is not the case since it is due to the external action carried out by the operator of the furnace to reposition the three lasers responsible for measuring the quantities on a central position of the specimen surface; this fact will also be encountered in subsequent experiments with this furnace.

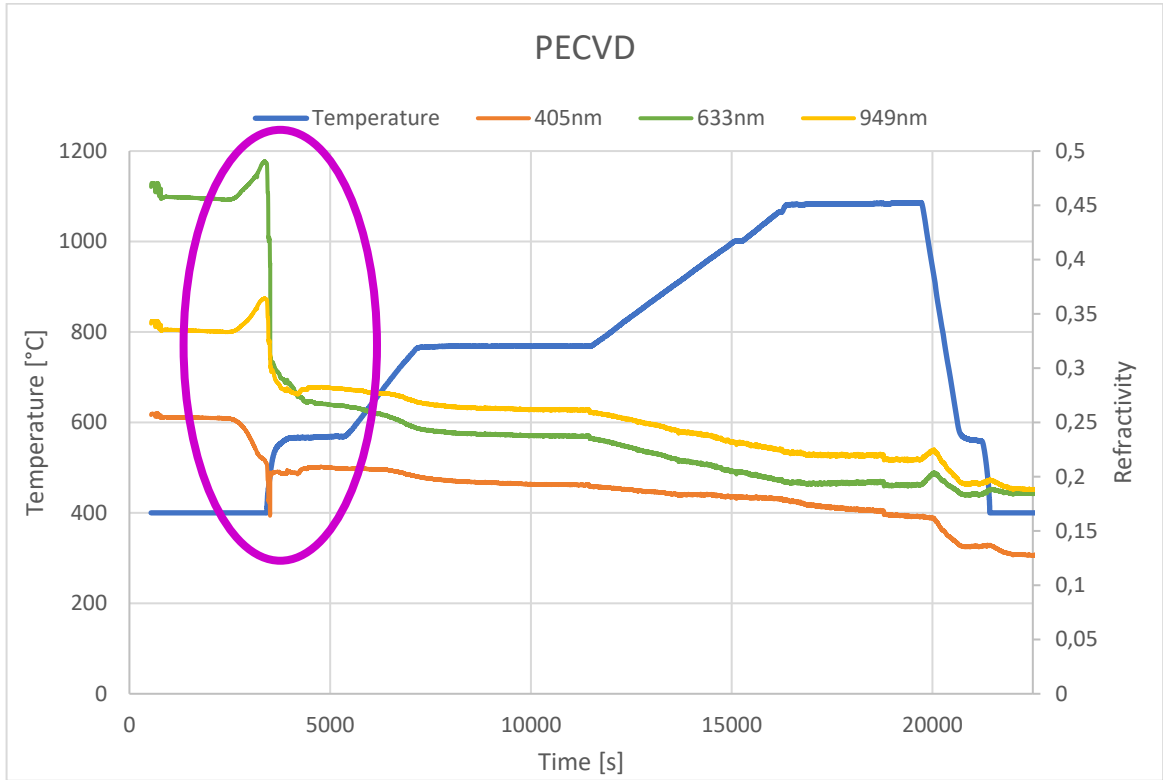


Figure 20: Refractivity in-situ measurements during the heat treatments for the PECVD sample.

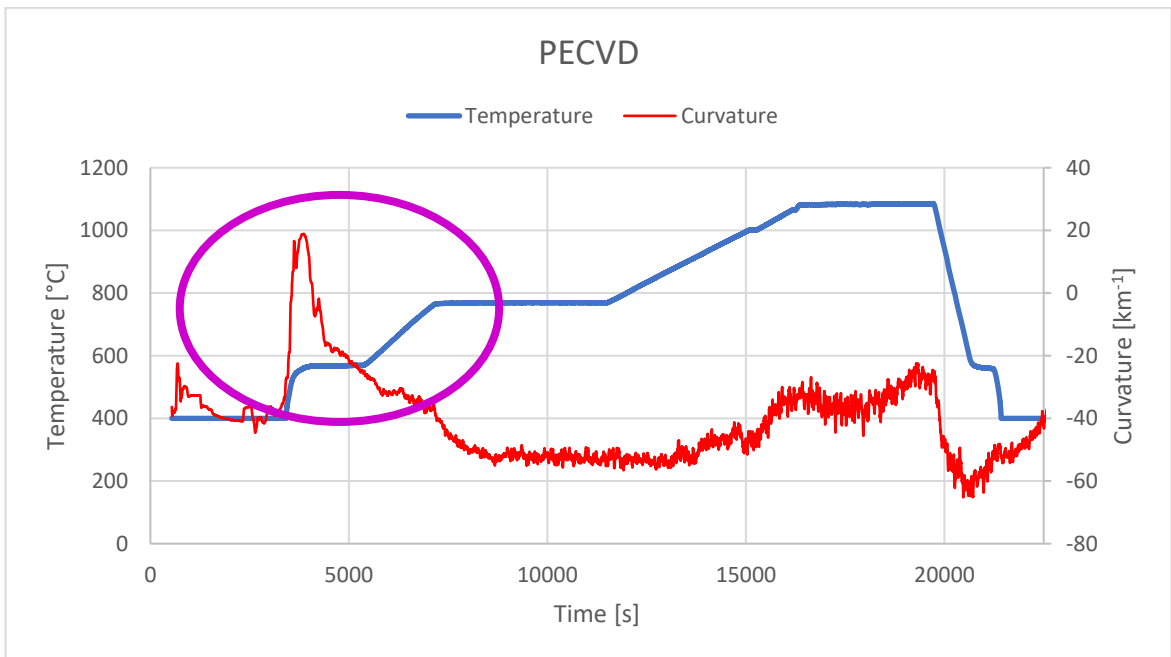


Figure 21: Curvature in-situ measurements during the heat treatments for the PECVD sample.

Thanks to this experiment, it was possible to identify that the delamination of the layer of this test specimen takes place at around 500°C, which obviously prevents any type of annealing or possibility of recrystallisation.

Furthermore, using the Stoney equation, from the recorded curvature values it is possible to calculate approximately the value of residual stresses within the SiC layer deposited. From this calculation, which in our case is considered only qualitative because it is very approximate since our layer is actually composed of two thin films (SiC + SiO₂), it is possible to deduce, however, that it is not a problem of internal stress and residual stress as the value is very far from the yield strength of the material itself in consideration.

Having ruled out a possible degradation reaction since the phenomenon occurs at low temperature, the problem could stem from a weak interfacial bond between the SiC and SiO₂ layers. To demonstrate this, a new experiment was set up using a third furnace less sophisticated: the heat treatment was carried out at T=450°C at atmospheric pressure in air for about 6 hours. The result obtained was a partial delamination of the specimen which made it possible to clearly identify the different phases of the process itself, thus confirming the hypothesis of low interfacial resistance between the two layers.

As can be seen in *Figure 22*, in some areas of the SiC layer (pinkish colour in the figure), it starts to crack and lift (a), creating a sort of bubble (blue area); then it peels off completely (b), leaving the SiO₂ uncovered (green area). The succession of these phenomena at a higher temperature leads to the complete delamination of the layer.

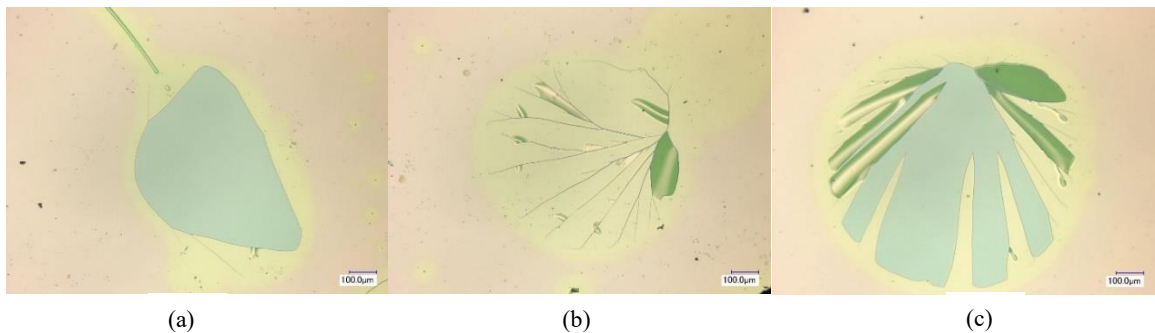


Figure 22: Surface of the PECVD sample shows the presence of a local layer detaching (a) and removing (b), and two different zones together (c) which could be the intermediate phenomenon step.

In order to continue the experiments with the silicon carbide layer deposited by the PECVD technique, this problem of delamination at low temperature must be solved: in general, the recrystallisation phenomenon of SiC definitely occurs above 1000°C. For example, one idea would be to functionalise the silica surface before deposition to improve the interfacial bonding.

3.2.2 PVD samples

In this section will be described and analysed the heat treatments carried out on the samples deriving from the wafer 2 and wafer 3; the *Table 8* is reported as a summary to visualise all the experiments done.

In this case, by performing annealing at 1300°C under vacuum, the silicon carbide layer did not undergo any delamination process; to confirm this experimentally, XPS and ellipsometry were carried out again.

PVD	Temperature	Pressure	Atmosphere	Time	Note
Annealing	T=1300°C	2 mbar	Vacuum	1 h	x
In-situ measurement LP Wafer 2	T=1080°C Plateau T=1120°C short plateau	3 mbar	Vacuum	About 1 hour the first plateau	Event about 960°C in the curvature values
In-situ measurement LP Wafer 3	T=1040°C Plateau	3 mbar	Vacuum	About 1 hour the first plateau	Event about 980°C in the curvature values
In-situ measurement HP Wafer 2	T=1170°C Plateau	500 mbar	Argon	About 1 hour the first plateau	Event about 1160°C in the curvature values
In-situ measurement HP Wafer 3	T=1150°C Plateau T=1185°C short Plateau	500 mbar	Argon	About 1 hour the first plateau	No event

Table 8: Heat treatments summary for the PECVD samples.

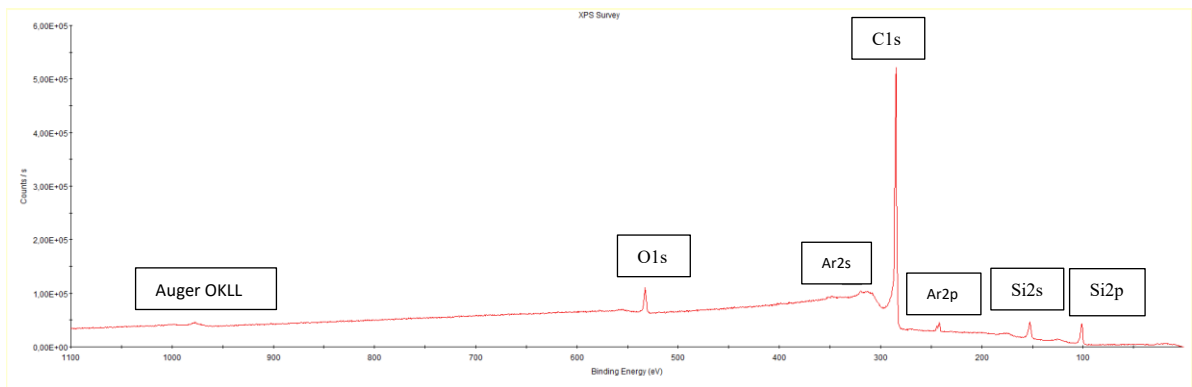
However, although no delamination occurred, the results obtained from the measurements carried out were not very positive: the XPS analysis reported a significant presence of C compared to Si (*Figure 23*) and therefore a prevalence of C-C bonds (*Figure 24*) with an increasing of C-H bonds.

In both samples, it was possible to note a shift in energy binding towards higher values of the C-Si bond (up to 283.7 eV) and the C-C bond (up to 284.6 eV) itself, as it can be seen in the *Table 9*. In addition, the strong presence of C is confirmed after 1-minute argon etching, ruling out surface contamination caused by the container and support of the graphite specimens. From these two considerations, it is possible to assume that a degradation reaction has taken place reducing the quantity of SiC and increasing the C in the layer, resulting in the graphitisation process of C itself.

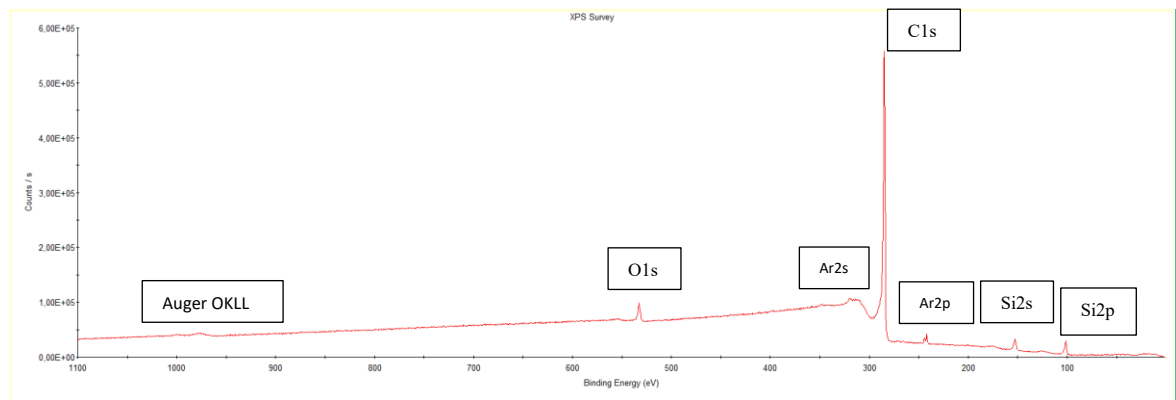
From the point of view of the silicon bonds, the results are not reported because the quantity is very low respect to the C respect to the usual system analysed so far.

PVD		
C1s		
Chemical Bond	Binding Energy (eV)	FWHM (eV)
C-Si	283.2±0.2	1.1±0.2
C-C	284.6±0.1	1.2±0.1
C-H	285.4±0.2	1.5±0.3
C-O	286.4±0.2	1.5±0.3

Table 9: Carbon binding energy reference table for PVD annealed samples.

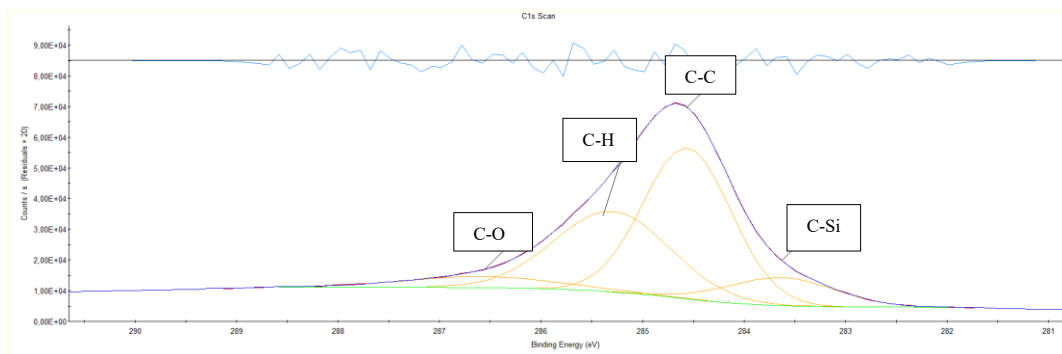


(a)

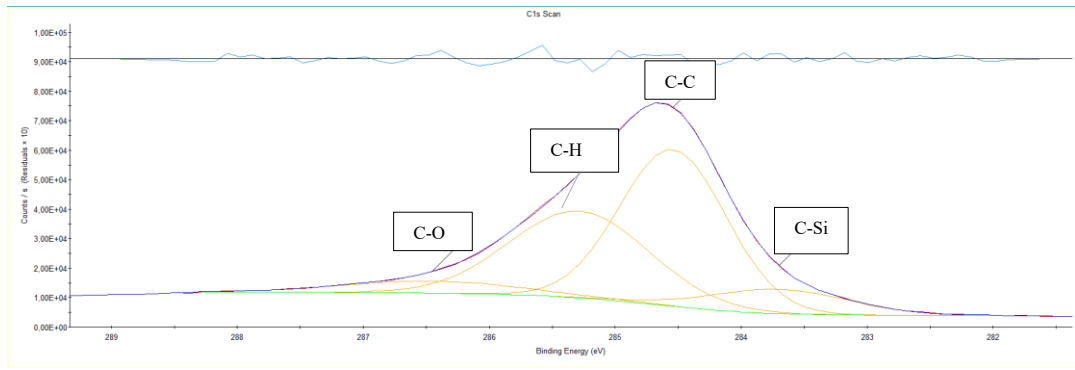


(b)

Figure 23: XPS survey after Ar etching of the 1300°C annealed PVD sample from wafer 2 (a) and from wafer 3 (b).



(a)



(b)

Figure 24: XPS results for C1s scan from the PVD wafer 2 (a) and 3 (b) after etching.

The evolution of the system in both samples is also confirmed by the ellipsometry as, by re-phasing the experimental data with both Tauc-Lorentz or Cody-Lorentz laws, it was not possible to obtain an acceptable result. Although the insertion of a carbon layer improves the fitting quality, the accuracy value is far from acceptable: for this reason, the optical experimental analysis of these two specimens will not be reported.

A Raman spectroscopy was then carried out to assess the possible presence of a crystalline SiC phase. However, the result obtained, shown in *Figure 25*, does not show a substantial change about the SiC, but rather what has undergone a clear difference is the carbon zone (start of separation into two different peaks), confirming an initial graphitisation process.

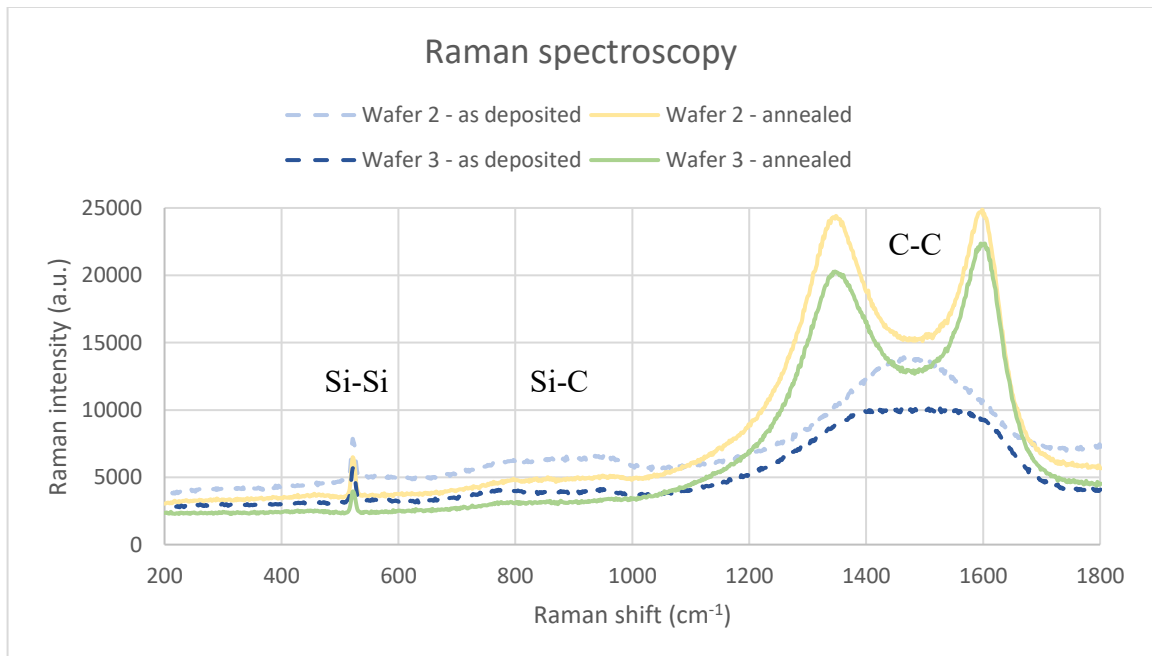
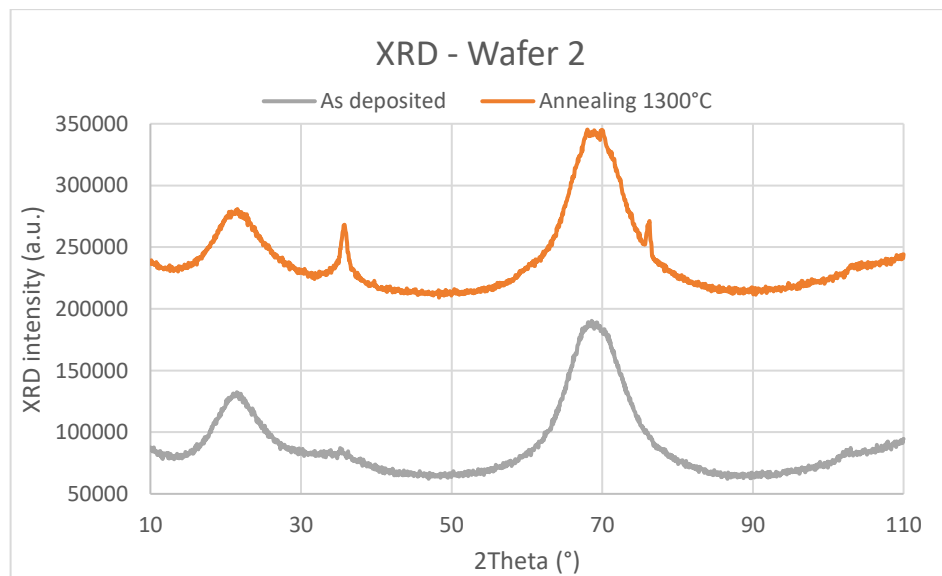


Figure 25: Raman spectroscopy for the PVD samples after annealing at 1300°C in comparison with the as deposited ones.

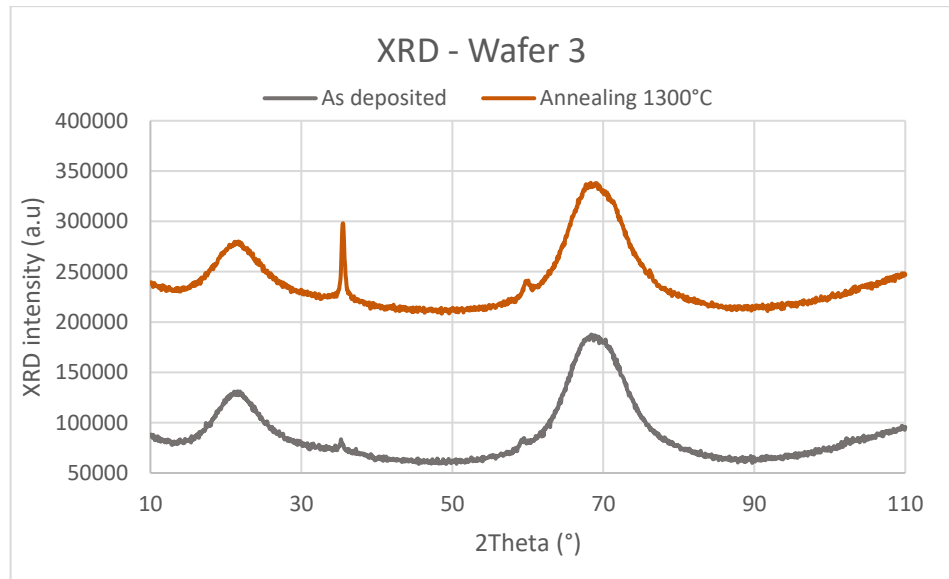
At this point, it was assumed that the very thin thickness of the SiC layer and the confirmed presence of C (as can be seen from the graph, an element that is very sensitive to this experimental measurement) could influence the negative Raman spectroscopy result on the recrystallisation process, as the temperature was high enough to activate the process. In order to assess the veracity of the above, a measurement was made using the XRD technique (using a geometry with an offset of 3°). Obviously, a preliminary analysis has been made on the as deposited SiC layer to evaluate any differences in the two spectra (*Figure 26*); moreover, it has been measured also the starting wafer to locate the amorphous silicon oxide peak, coming from the $2\ \mu\text{m}$ thermal grown layer (around 21°), and the well-known silicon (100) peak, mainly coming from the substrate (around 69.9°).

From this measurement it has been possible to appreciate the occurrence of a crystalline silicon carbide phase in both specimens: although traces are already present in the specimen, after annealing the main SiC contribution [111] around 35.5° is clearly visible. Furthermore, it is possible to notice the peak at around 60° (in sample from the wafer 3) and at around 76° (in the other one).

As can be seen from *Figure 27*, it is possible to assume a SiC-3C crystalline phase which is the most common: as not all the main peaks are present (some hidden within the silicon peak itself) it is not possible to conclude it with certainty. However, the fact that some peaks are not present could be traced back to a crystalline phase preferentially oriented along a certain direction.



(a)



(b)

Figure 26: XRD measurements before and after annealing at 1300°C of samples from wafer 2 (a) and wafer 3 (b).

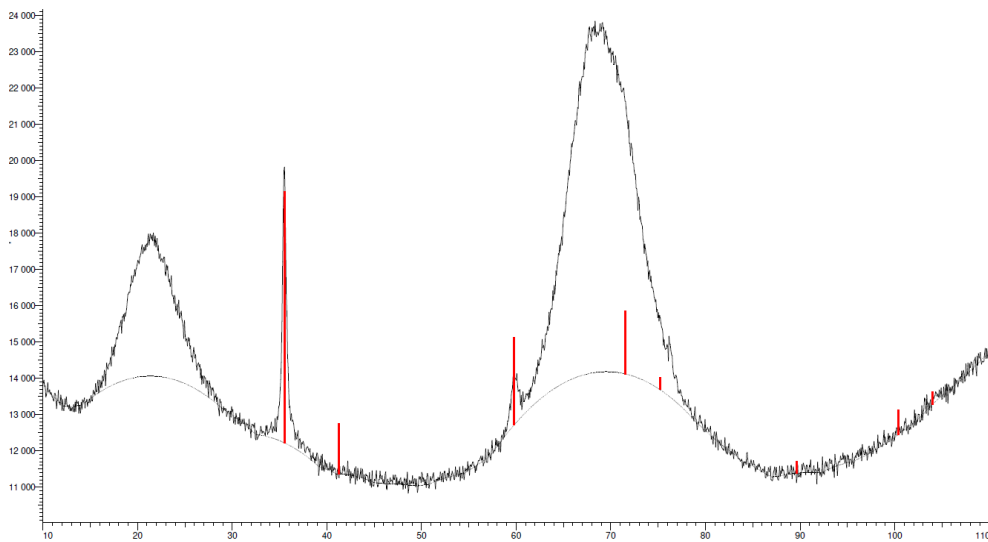


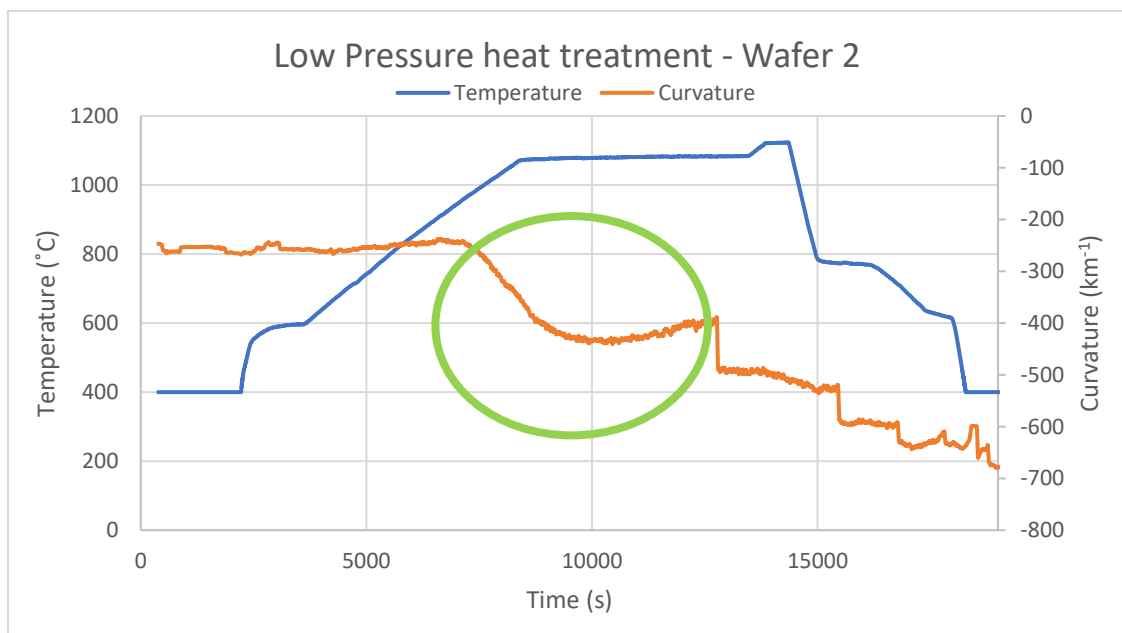
Figure 27: SiC-3C phase XRD peaks correspondence, matching the sample from the wafer 3 after annealing at 1300°C.

Although partial recrystallisation of the layer occurred at 1300°C, surface degradation also occurred at this temperature as a C layer formed; this problem needs to be resolved as a silicon carbide layer is required for this application and it is not acceptable to have a degraded surface.

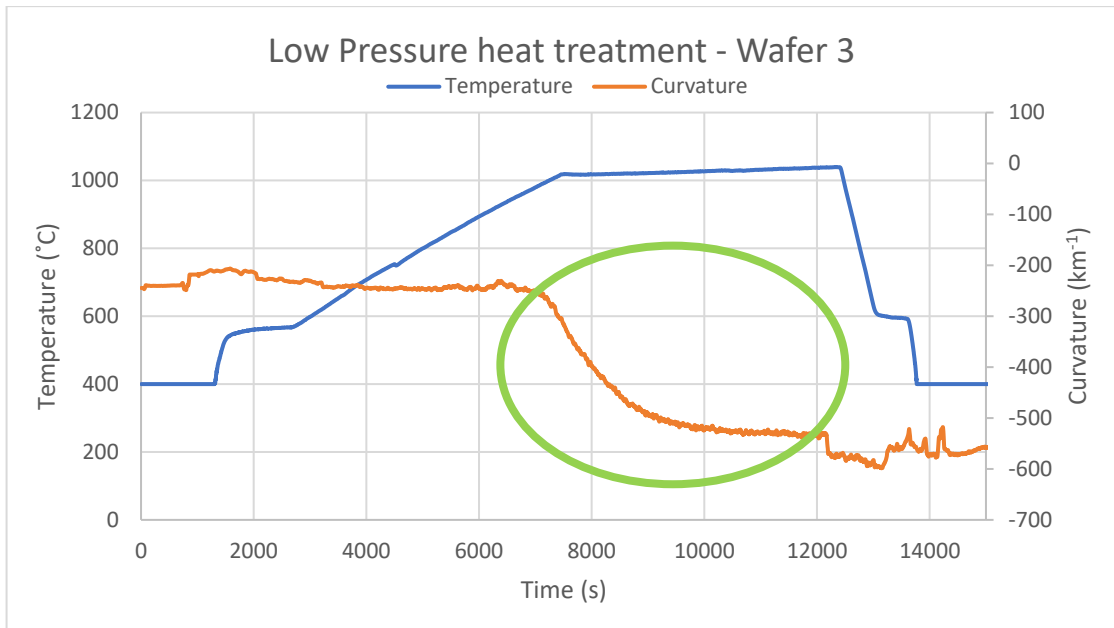
At this point it was decided to carry out two in-situ measurements for both samples (wafer 2 and wafer 3) in order to try to identify the temperature (combined with the pressure) at which this degradation phenomenon occurs.

As mentioned in *Table 8*, the heat treatments performed differ mainly in the pressure at which they were carried out and in the temperature at which the thermal stop was performed.

In particular, the low-pressure treatment (LP) was carried out in a vacuum at about 3 mbar (minimum furnace limit), while the "high-pressure" treatment (HP) was carried out at 500 mbar in an argon atmosphere. As regards the temperatures, however, in all cases they were the about the maximum attainable by the furnace (it was controlled by the current passing through the graphite resistance modifying the voltage applied value): the temperature varies since it is measured on the surface of the sample and therefore depends on the thickness of the layer itself (and the whole sample), but above all on whether there is a convective component given by the gas or not. The maximum temperature attainable for each system was therefore variable and could not be precisely predicted a priori: in heat treatments wafer 2 LP and wafer 3 HP, the two plateaus were carried out because, once the first one had been carried out, it was possible to increase the temperature further and check if any phenomena occurred. To summarise, the maximum temperatures reached during heat treatments are as follows: 1120°C at low pressure and 1170°C at “high pressure” for the wafer 2’s samples, and 1040°C at LP and 1185°C at HP for the wafer 3 ones.



(a)



(b)

Figure 28: Curvature in-situ measurements during the LP heat treatments for the PVD samples of wafer 2 (a) and 3 (b).

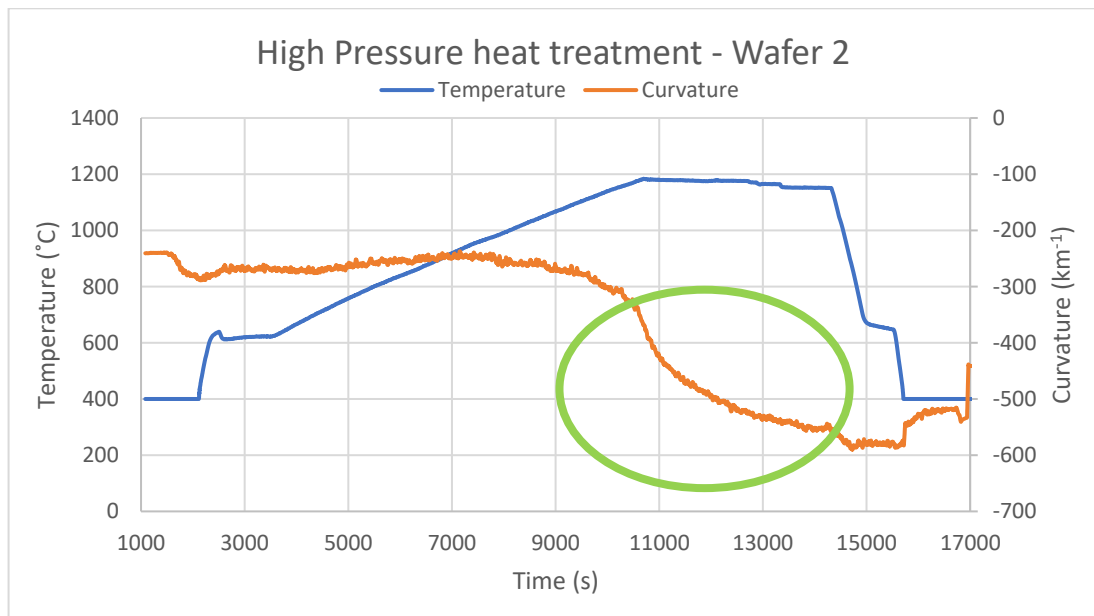


Figure 29: Curvature in-situ measurements during the HP heat treatments for the PVD samples of wafer 2.

From the result of the in-situ measurements, it could be seen that for all four specimens there was no abrupt change in refractivity during all experiments for all 3 wavelengths; this suggests that the SiC film did not undergo any degradation phenomenon, as if a carbon layer had formed on the surface, changes would most likely occur. However, in three out of four an abrupt change in the value of the curvature was recorded at about 960°C-980°C for LP annealing (Figure 28) and at about 1160°C for HP ones (Figure 29): the event shifts to higher

temperatures when higher pressure was used, so that in the case of wafer 3 it could not be recorded.

As mentioned above in the case of the PECVD specimen, all other sudden variations (which do not follow the temperature trend) are determined by the external action of the operator to reposition the three lasers on the surface of the sample.

This phenomenon found on the curvature, not being recorded also in the measurement of refractivity, only suggests an internal reorganisation of the layer: there is an internal contraction leading to a final curvature value greater than the initial one. One explanation could be the recrystallisation phenomenon as it leads to an internal packing of the atoms and a consequent increase in the young modulus E .

However, the XRD analysis (*Figure 30* and *Figure 31*) shows that not only the first three specimens underwent recrystallisation (always with the assumed crystalline SiC-3C phase), but also the fourth specimen, which casts doubt on whether the phenomenon recorded can be attributed with certainty to the recrystallisation of silicon carbide. It would be worthwhile to carry out several experiments of this kind to verify whether the event recorded in the curvature data can be attributed to a certain 'amount' of crystalline (re-crystallised) phase and not to the actual onset of the phenomenon, or whether it is possibly another phenomenon and what it is.

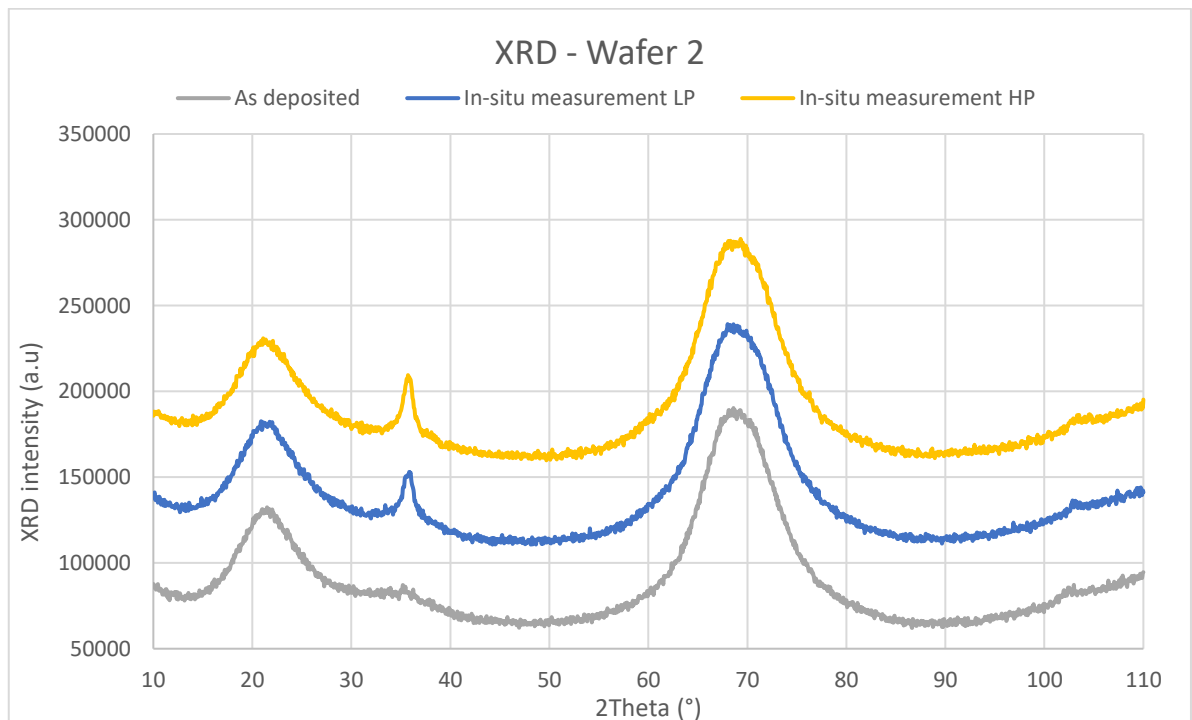


Figure 30: XRD measurements before and after heat treatments of PVD samples from wafer 2.

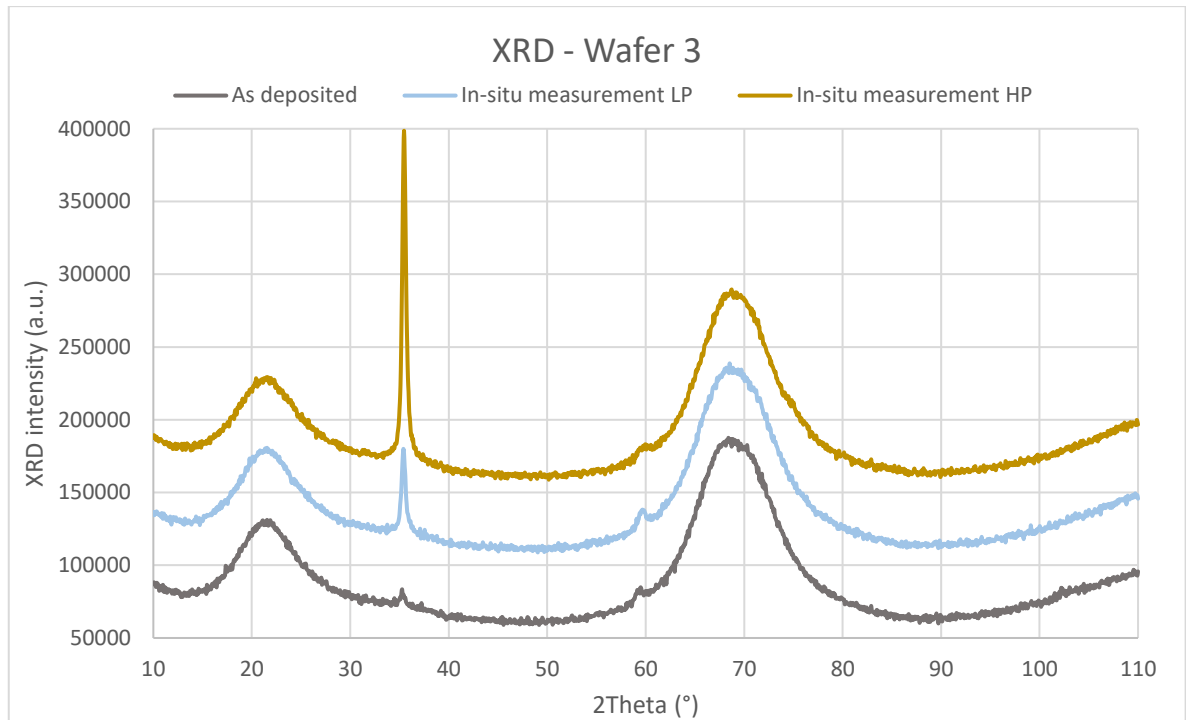


Figure 31: XRD measurements before and after heat treatments of PVD samples from wafer 3.

Focusing on the SiC [111] contribution (around 35.5°), both the peak height and the peak profile change from one sample to another; large peak profiles are mainly related to lower crystallite size (or low quantity phase) and it is expected to see thinner peak profiles and higher intensities after a heat treatment (but the quantity is related on the integrated area of the peak). Indeed, this evolution is what it has been found analysing all XRD results before and after annealing or in-situ heat treatment experiments.

For what concern the XPS measurement, it ascertained that no surface degradation had occurred: the situation of the as-deposited specimens was essentially the same, both about the ratio of C-Si and C-C bonds and the position of the characteristic peaks. Although the layer does not seem to have changed its chemical structure, the ellipsometry showed that the samples underwent a change in the optical properties: the refractive index and the extinction coefficient are modified after the "high pressure" heat treatments. Indeed, in the case of wafer 2 the values of $n=2.63$ and $k=0.1$ were reached, while for wafer 3 the values of $n=2.67$ and $k=0.13$ were reached; the gap of difference of both values between the two wafers narrowed. As in the previous cases, no recrystallisation within the layer could be identified by Raman spectroscopy (Figure 32). However, it should be noted that no significant evolution of the "C-C phase" was found, although a beginning of peak separation is visible.

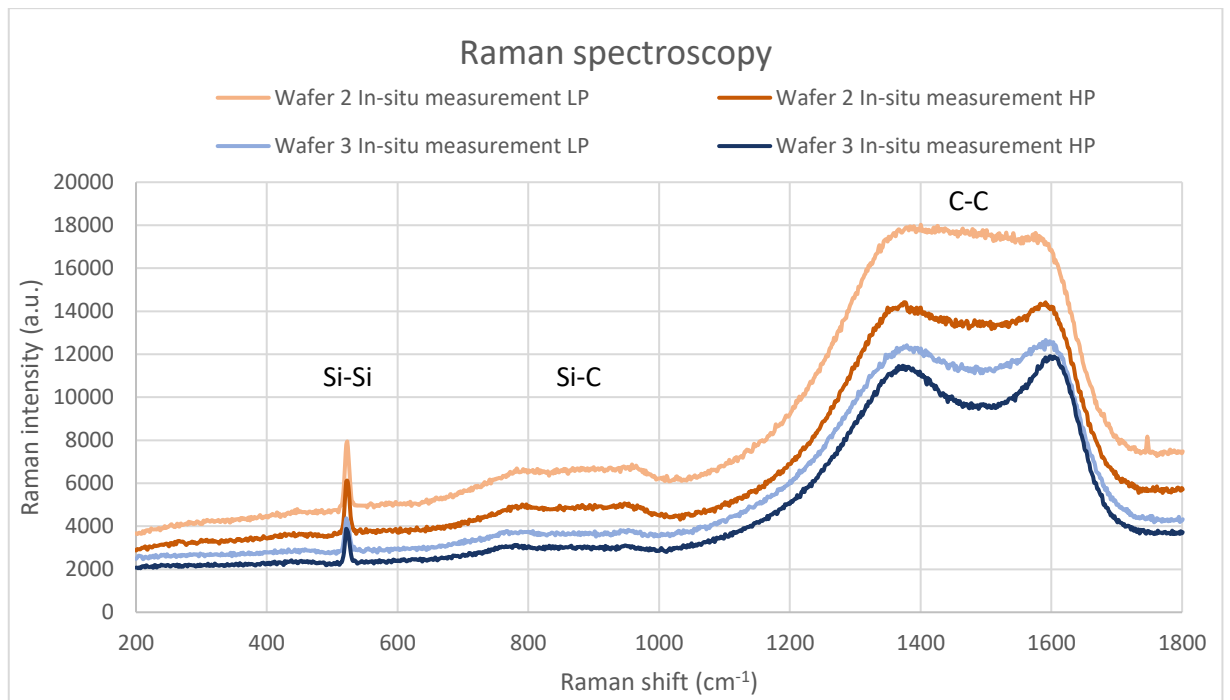


Figure 32: Raman spectroscopy for the PVD samples from wafer 2 and 3 after the different heat treatments LP and HP.

So, although there are still many aspects to be analysed and understood, about both PVD specimens it seems that we are on the right track to be able to study and experiment with layer recrystallisation. Clearly, much more time and experiments will be needed to get the full picture of the system under investigation.

Chapter 4: Analysis and discussion of results

One of the aims of the European project to which the internship is related is to deposit a 500 nm film of amorphous silicon carbide at low temperature and then recrystallize it. In order to meet this requirement, two deposition techniques were used: PECVD and PVD.

Although the deposition was successful and the homogeneity was more than acceptable, the thickness of the layer is one aspect that should be improved; with PECVD deposition, a thickness of around 350nm was achieved, while with PVD around 600nm was achieved in both cases (590nm and 605nm to be precise). Another detail to be taken care of is the contamination of the layer, since in wafer 1 there was a presence (not only superficial) of nitrogen and boron, while in wafers 2 and 3 there was chlorine and argon.

The solution to these problems is, of course, just to make several depositions by changing the deposition parameters to find the optimum values to minimise contamination and obtain a layer with a thickness as close as possible to 500 nm. However, these details did not indicate any problems with the experiments carried out, as they are aspects that may need to be refined later as they do not significantly affect the system studied, the main aim being recrystallisation.

As seen, several experimental measurements were carried out to accurately characterise the different layers deposited. The combination of Raman and X-ray Photoelectron spectroscopies produced some very interesting results from the chemical point of view and from the organisation of the atoms/bonds within the SiC film. Indeed, it has been found that there are both areas in which carbon is bound with silicon and areas in which it is bound with itself, with a considerable and not negligible ratio of quantities; as if the layer were made up of two different phases: C and SiC. In addition, the silicon carbide 'phase' must be clearly rich in silicon, as the layer must be almost stoichiometric in its entirety. Although from Raman spectroscopy it is not possible to discriminate Si-Si bonds exclusively in the layer because the signal from the substrate itself is present, even from the XPS measurement the characteristic peaks of Si-Si (and Si-H) bonds are not clearly evident.

However, it has been noted that the energy binding characteristic of Si-C bonding (so from the point of view of the silicon spectrum) shifts towards lower values: the hypothesis is that because the Si-Si and Si-H bonds have lower energy binding (about 99.2 eV) than the Si-C bonds, and because they are part of the same 'phase' within the material, they shift the main peak to lower values, without causing all the characteristic peaks to occur. Indeed, if looking

closely at the hypothesised chemical structure, and since the layer is amorphous (disordered structure), it is possible that a Si atom is not only bound to C atoms (statistically the most present), but also to atoms of silicon itself and of hydrogen when present. For this reason, it could be that from the XPS analysis we only see the main Si-C peak shifted to lower binding energies as the other two bonds are also included, as if it were a kind of total average from different contributions. This would explain the fact that there is no direct presence of hydrogen in the layer deposited with the PECVD technique; another aspect that supports the hypothesis made is that the binding energy of the Si-C bond in wafer 1 (PECVD) is lower than in wafers 2 and 3 (PVD) (100.1 eV vs 100.6 eV): the contributions to lowering the binding energy of the main peak are two, Si-Si and Si-H, while in the other cases only Si-Si. With the PVD technique, the deposition does not take place via a chemical reaction of hydrogen-containing gases, so no hydrogen is expected to be present in the SiC film. Obviously, in order to affirm and prove this hypothesis, numerous experiments and measurements must be carried out so that the whole system under analysis can be understood and explained.

The fact that the deposited layer can be imagined as two different phases (carbon + silicon rich SiC) also has a considerable impact on the recrystallisation aspect, as this can only take place partially. In order to have the film recrystallisation as homogeneously as possible, diffusion treatments could be carried out so that the SiC is actually mainly present. This aspect will also have to be subjected to numerous experimental tests to assess its possibility and effectiveness.

Moreover, from the ellipsometry measurements it has been confirmed that the PECVD sample contains hydrogen due to the very low refractive index ($n=2.32$) compared to the literature value for the SiC.

After all the characterisations of the wafers had been carried out and the SiC layers deposited, the various heat treatments were carried out in order to begin to study the possible recrystallisation phenomenon.

It was found that specimens deposited using the PECVD technique undergo delamination at around 500°C, making it impossible to carry out any kind of study at high temperatures, as is required for recrystallisation.

Analyses have shown that this is probably a problem of adhesion between the silicon carbide layer and the thermally grown silica layer on the wafer surface. Therefore, for example, surface preparation using primers should be carried out before deposition.

Although the PVD specimens did not experience any delamination problems during all the heat treatments performed, a degradation phenomenon occurred when the annealing at 1300°C under vacuum for one hour has been done, for both types of PVD samples; experimental analysis revealed the presence of an exclusively C surface layer, partially graphitised. Subsequent heat treatments were carried out at a lower temperature and varying pressure, with in-situ measurements taken to detect any phenomena during the experiments: despite abrupt changes in curvature were detected, no degradation or delamination occurred, suggesting an internal reorganisation of the layer itself.

The XRD technique has been used to check for the possible presence of a crystalline phase, as nothing could be detected by Raman spectroscopy measurements: this was probably due to the thickness of the layer and the presence of the C-C 'phase', which presents a significant signal. The results show that, in all PVD specimens after any heat treatment, a crystalline phase is identified that is probably attributable to the more common SiC-3C. Indeed, there is a main SiC [111] contribution at about 35.5° and two secondary peaks at 60° and 76°. Nevertheless, as not all the main peaks are present (some hidden within the silicon peak itself) it is not possible to conclude it with certainty, but this fact could be traced back to a crystalline phase preferentially oriented along a certain direction.

Focusing on the SiC [111] contribution, both the peak height and the peak profile change from one sample to another; large peak profiles are mainly related to lower crystallite size (or low quantity phase) and it is expected to see thinner peak profiles and higher intensities after a heat treatment (but the quantity is related on the integrated area of the peak). Indeed, this evolution is what it has been found analysing all XRD results before and after annealing or in-situ heat treatment experiments.

Obviously, all this is only a starting point, as has already been stated several times, of a very long experimental path; even with regard to heat treatments and XRD measurement, several experiments will have to be carried out in order to determine what are the optimal parameters of temperature, time and pressure to obtain a good recrystallisation of the layer and which crystalline phase is achieved. Furthermore, it will be useful to understand how and how much these parameters affect the percentage of crystallinity, size and directionality of the crystalline phase itself.

Chapter 5: Conclusions

During the internship, based on a European project, several experiments and experimental measurements were carried out to characterise an amorphous SiC film deposited at low temperature, by PECVD or PVD, on a 2 μm thick SiO₂ layer grown on a silicon wafer (100). Various heat treatments were carried out to study the possible recrystallisation of the film itself.

Starting with the deposition itself, the objectives about the thickness of the SiC layer were not perfectly achieved; in fact, although the request was for 500 nm, with PECVD the thickness obtained was around 350 nm, while with PVD it was around 600 nm in both cases. Furthermore, another aspect to be considered and which should be improved concerns the contamination deriving from the production processes. Although the purity of the film was high enough to carry out the experiments, given the final application in the optical field it must be optimized as much as possible.

From the chemical analysis and organisation of the samples, it can be assumed that the silicon carbide should be organised in two different phases: carbon + silicon rich SiC; this was found by Raman and X-ray Photoelectron spectroscopies.

Once the heat treatments were carried out, two main problems were encountered: the layer deposited using the PECVD technique undergoes a delamination at about 500 °C (probably determined by a weak adhesion bonding) making any type of study on the phenomenon of recrystallization impossible, while those through the PVD undergo a degradation process at 1300 °C for one hour under vacuum. Despite the first is a problem deriving from the production process, the second will become the object of study and experimentation to understand it, explain it and be able to avoid it.

However, by lowering the temperature (about 1100°C-1200°C), it was possible to record a partial recrystallization of the silicon carbide, without undergoing degradation phenomena. Although it is not possible to declare it with certainty given the lack of some characteristic peaks (some superimposed on those of silicon), the crystalline phase present should be the common SiC-3C given the presence of peaks at 35.5°, 60° and 76°. It is important to underline that this fact could derive from a preferential directionality of the crystalline phase. Clearly all the work done is a first step of a long journey. In addition to improving the deposition and studying the phenomena found (degradation and delamination), it will be necessary to conduct multiple experiments to fully define the chemical structure of the SiC

amorphous film, the recrystallization process by varying parameters such as temperature, pressure and time.

A final aspect that could be studied in the future is the possibility and effectiveness of inserting a diffusion process, previous or subsequent to the various heat treatments to ensure that the final recrystallized layer is mainly composed of SiC.

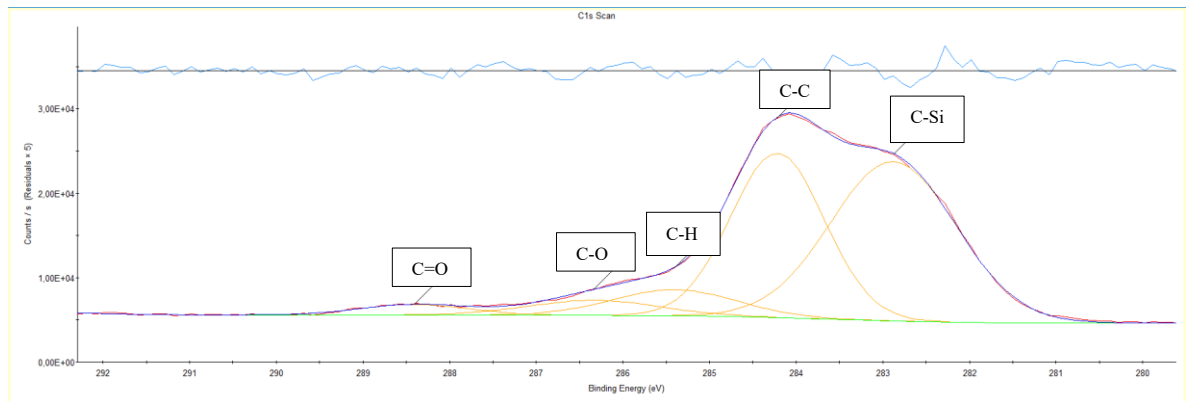
Bibliography

- [1]: FRISCHMUTH, Tobias, et al. High temperature annealing effects on the chemical and mechanical properties of inductively-coupled plasma-enhanced chemical vapor deposited a-SiC: H thin films. *Thin Solid Films*, 2016, 611: 6-11.
- [2]: RICCIARDI, C., et al. Microstructure analysis of a-SiC: H thin films grown by high-growth-rate PECVD. *Journal of non-crystalline solids*, 2006, 352.9-20: 1380-1383.
- [3]: SUMMONTE, C., et al. Wide band-gap silicon-carbon alloys deposited by very high frequency plasma enhanced chemical vapor deposition. *Journal of applied physics*, 2004, 96.7: 3987-3997.
- [4]: JANZ, Stefan. *Amorphous silicon carbide for photovoltaic applications*. 2006. PhD Thesis.
- [5]: PETRIK, Peter; RACZ, Adel Sarolta; MENYHARD, Miklos. Complementary physicochemical analysis by ellipsometry and Auger spectroscopy of nano-sized protective coating layers. *Applied Surface Science*, 2020, 534: 147593.
- [6]: CALCAGNO, L., et al. Crystallisation mechanism of amorphous silicon carbide. *Applied surface science*, 2001, 184.1-4: 123-127.
- [7]: CONTARINI, S., et al. XPS study on the dispersion of carbon additives in silicon carbide powders. *Applied surface science*, 1991, 51.3-4: 177-183.
- [8]: ERNST, K.-H., et al. XPS study of the a-C: H/Al₂O₃ interface. *Surface and interface analysis*, 1994, 21.1: 32-37.
- [9]: INOUE, Y., et al. Raman spectra of amorphous SiC. *Solid state communications*, 1983, 48.12: 1071-1075.
- [10]: KUENLE, Matthias, et al. Thermal annealing of SiC thin films with varying stoichiometry. *Materials Science and Engineering: B*, 2009, 159: 355-360.
- [11]: MATSUNAMI, Hiroyuki; MASAHIRO, Hagio; TANAKA, Tetsuro. Structures and physical properties of sputtered amorphous SiC films. *Journal of Electronic Materials*, 1979, 8.3: 249-260.
- [12]: MONACO, Gianni, et al. Optical constants of silicon carbide deposited with emerging PVD techniques. In: *EUV and X-Ray Optics: Synergy between Laboratory and Space*. International Society for Optics and Photonics, 2009. p. 73600W.
- [13]: NGUYEN, N. V.; VEDAM, K. Spectroscopic ellipsometry studies of crystalline silicon implanted with carbon ions. *Journal of applied physics*, 1990, 67.8: 3555-3559.
- [14]: TERSOFF, J. Chemical order in amorphous silicon carbide. *Physical Review B*, 1994, 49.23: 16349.
- [15]: ZOLLNER, Stefan, et al. Dielectric functions of bulk 4H and 6H SiC and spectroscopic ellipsometry studies of thin SiC films on Si. *Journal of applied physics*, 1999, 85.12: 8353-8361.
- [16]: FITZGERALD, A. G., et al. Quantification of amorphous SiC: H films using XPS and AES with three standards. *Surface and interface analysis*, 1989, 14.6-7: 376-380.
- [17]: SWAIN, Bibhu P. The analysis of carbon bonding environment in HWCVD deposited a-SiC: H films by XPS and Raman spectroscopy. *Surface and Coatings Technology*, 2006, 201.3-4: 1589-1593.

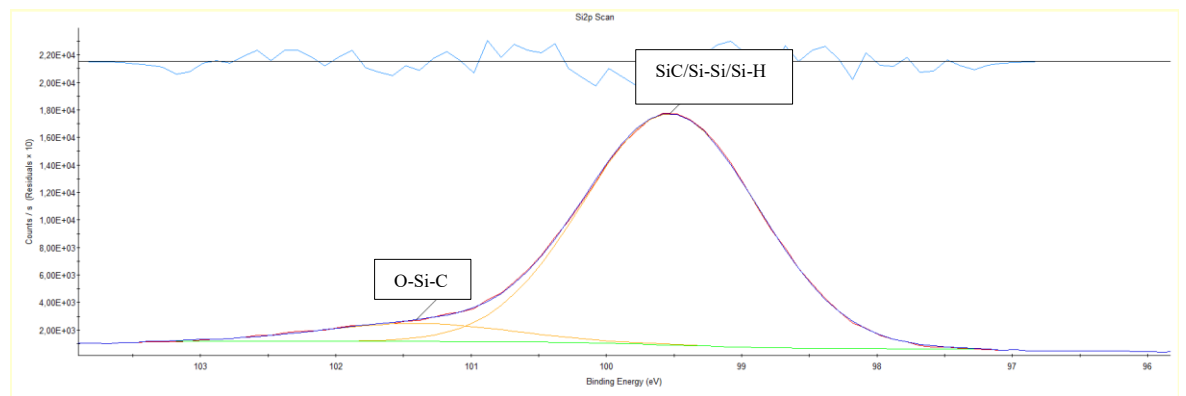
- [18]: CHOI, W. K., et al. Infrared and x-ray photoelectron spectroscopy studies of as-prepared and furnace-annealed radio-frequency sputtered amorphous silicon carbide films. *Journal of applied physics*, 1998, 83.9: 4968-4973.
- [19]: WANG, Y.-Y.; KUSUMOTO, K.; LI, C.-J. XPS analysis of SiC films prepared by radio frequency plasma sputtering. *Physics Procedia*, 2012, 32: 95-102.
- [20]: CHEN, Enlong, et al. RF-PECVD deposition and optical properties of hydrogenated amorphous silicon carbide thin films. *Ceramics International*, 2014, 40.7: 9791-9797.
- [21]: DELPLANCKE, Marie-Paule, et al. Preparation and characterization of amorphous SiC: H thin films. *Journal of Vacuum Science & Technology A: Vacuum, Surfaces, and Films*, 1991, 9.3: 450-455.
- [22]: RAJAGOPALAN, T., et al. Low temperature deposition of nanocrystalline silicon carbide films by plasma enhanced chemical vapor deposition and their structural and optical characterization. *Journal of Applied Physics*, 2003, 94.8: 5252-5260.
- [23]: TABATA, A., et al. X-ray photoelectron spectroscopy (XPS) of hydrogenated amorphous silicon carbide (a-SiC_{1-x}:H) prepared by the plasma CVD method. *Journal of Physics D: Applied Physics*, 1990, 23.3: 316.
- [24]: SERRE, Christophe, et al. Ion-beam synthesis of amorphous SiC films: structural analysis and recrystallization. *Journal of applied physics*, 1996, 79.9: 6907-6913.
- [25]: TEHRANI, F. Shariatmadar. Transformation from amorphous to nano-crystalline SiC thin films prepared by HWCVD technique without hydrogen dilution. *Bulletin of Materials Science*, 2015, 38.5: 1333-1338.
- [26]: Pierson, Hugh O. *Handbook of chemical vapor deposition: principles, technology and applications*. William Andrew, 1999.
- [27]: Mattox, Donald M. *Handbook of physical vapor deposition (PVD) processing*. William Andrew, 2010.
- [28]: Sharma, Varun. "Spectroscopic ellipsometry for the in-situ investigation of atomic layer depositions." (2014).
- [29]: <https://www.nanoanalytics.com/en/services/techniques/x-ray-photoelectron-spectroscopy-xps.html>.
- [30]: Larkin, Peter. *Infrared and Raman spectroscopy: principles and spectral interpretation*. Elsevier, 2017.
- [31]: <https://en.wikipedia.org/wiki/Ellipsometry>.
- [32]: https://en.wikipedia.org/wiki/Brewster%27s_angle.
- [33]: Negara, Christian. "Fast polarization state detection by division-of-amplitude in a simple configuration setup." *Proceedings of the 2015 Joint Workshop of Fraunhofer IOSB and Institute for Anthropomatics, Vision and Fusion Laboratory*. Vol. 24. J. Beyerer and A. Pak (KIT Scientific Publishing, Karlsruhe, 2016), 2016.

Appendix

Wafer 1 surface



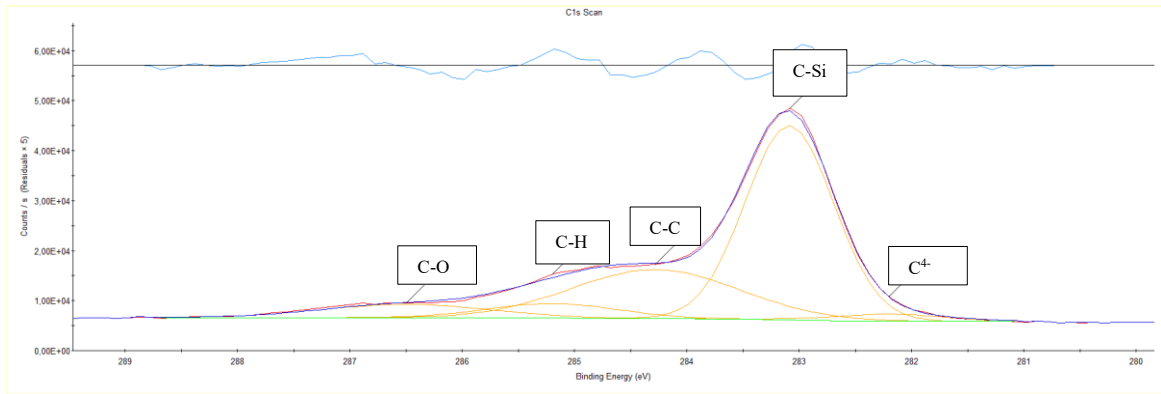
(a)



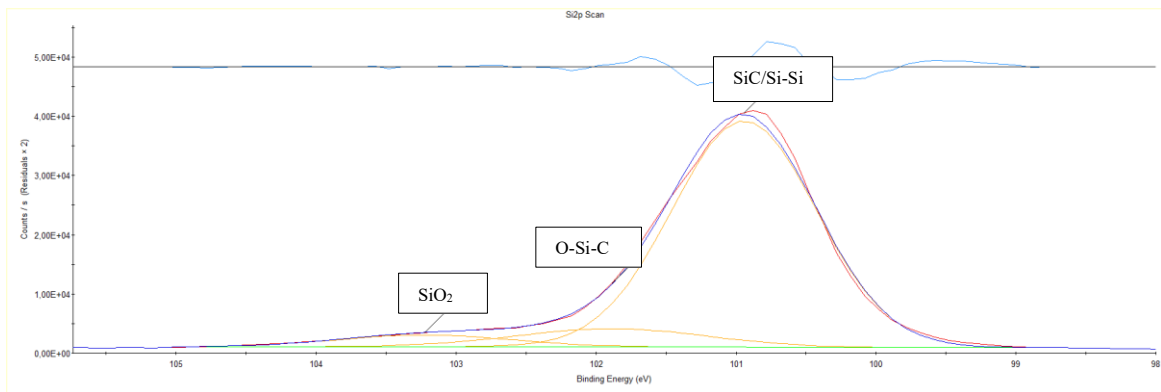
(b)

Figure 33: XPS results for C1s scan (a) and Si2p scan (b) from PECVD sample on the surface before Ar etching.

Wafer 2 surface



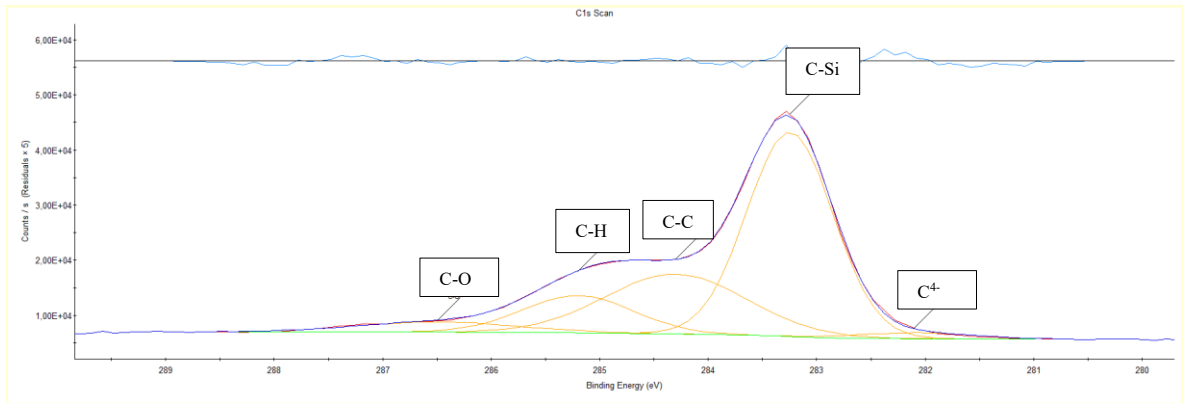
(a)



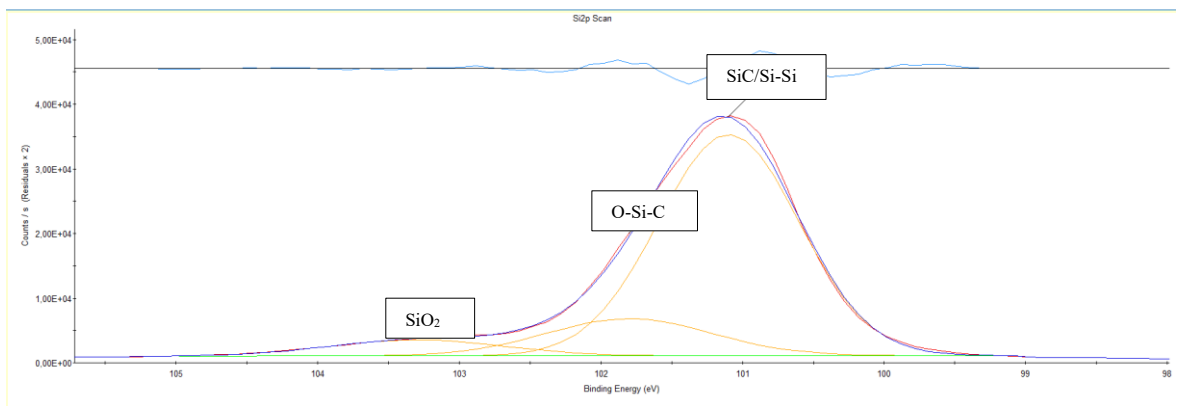
(b)

Figure 34: XPS results for C1s scan (a) and Si2p scan (b) from the PVD wafer 2 sample before Ar etching.

Wafer 3 surface



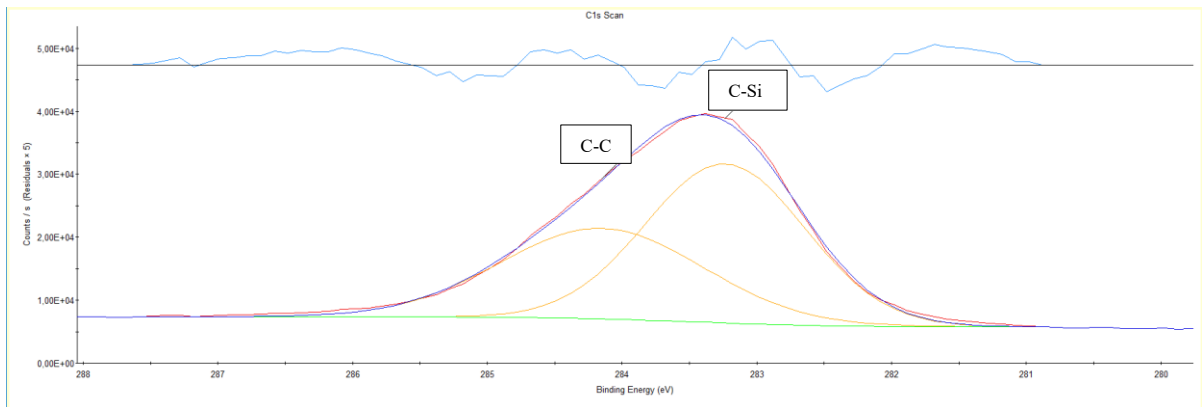
(a)



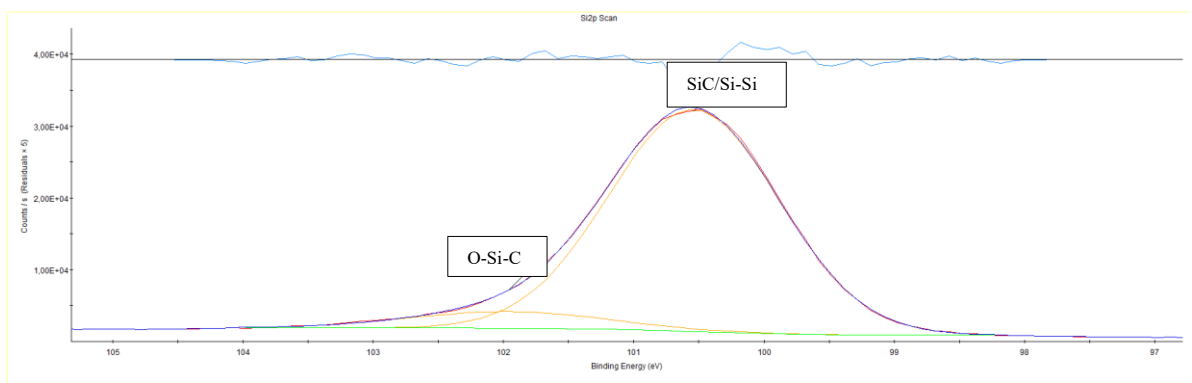
(b)

Figure 35: XPS results for C1s scan (a) and Si2p scan (b) from the PVD wafer 3 sample before Ar etching.

Wafer 3 after Ar etching



(a)



(b)

Figure 36: XPS results for C1s scan (a) and Si2p scan (b) from the PVD wafer 3 sample after Ar etching.

PECVD after heat treatments

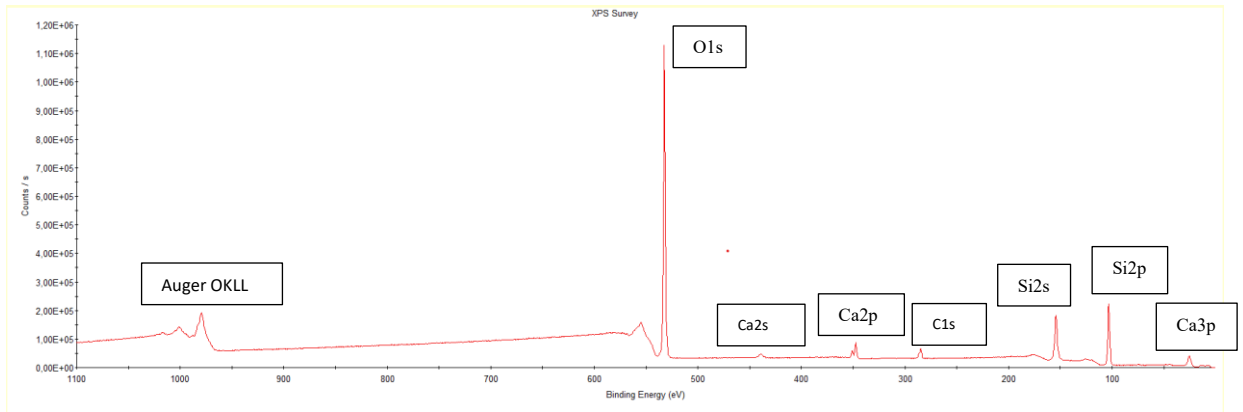


Figure 37: XPS survey before and after Ar etching of the annealed PECVD sample.

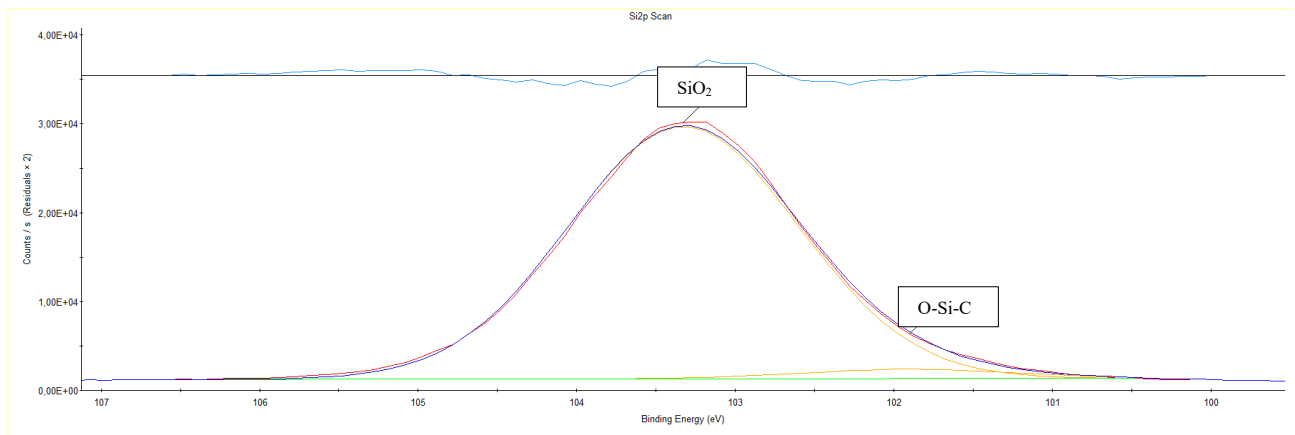


Figure 38: XPS results for Si2p scan for the PECVD annealed sample.